Schweizerische Eidgenossenschaft
Confédération suisse
Confederazione Svizzera
Confederaziun svizra

Federal Department of the Environment, Transport, Energy and Communications DETEC

Swiss Federal Office of Energy SFOE
Energy Research and Cleantech Division

Interim report dated April 2025

Demonstration of high-performance CO_2-selective graphene membranes for energy-efficient carbon capture

EfficientCapture

Source: ©Laboratory of Advanced Separations, EPFL; 2022

Location: Bern

Publisher:
Swiss Federal Office of Energy SFOE
Energy Research and Cleantech
CH-3003 Bern
www.bfe.admin.ch

Co-financing:

Subsidy recipients:
École Polytechnique Fédérale de Lausanne (EPFL)
Rue de l'Industrie 17, Case Postale 440, CH-1950 Sion

GAZNAT
Av. Général-Guisan 28, 1800 Vevey

Authors:
Prof. Kumar Varoon Agrawal, GAZNAT Chair of Advanced Separations, EPFL
kumar.agrawal@epfl.ch

SFOE project coordinators:
Men Wirz, Men.Wirz@bfe.admin.ch
Elena-Lavinia Niederhäuser, lavinia.niederhaeuser@bfe.admin.ch

SFOE contract number: SI/502268-01

Zusammenfassung

Die erfolgreiche Umsetzung des vom Schweizer Bundesrat gesetzten Netto-Null-Ziels erfordert eine rasche Entwicklung energieeffizienter Technologien zur CO_2-Abscheidung. Dieses Projekt baut auf der neuartigen zweidimensionalen (2D) Membrantechnologie der EPFL auf, bei der ein poröser Graphenfilm mit atomarer Dicke als CO_2-selektive Schicht verwendet wird. Ziel des Projekts ist es, die Technologie auf den Metermaßstab zu skalieren (Membranen im Quadratmeterbereich) und die Abscheidung von 1 kg CO_2 pro Tag zu demonstrieren.

Bisher wurden mehrere Maßnahmen eingeführt, die die Kosten für poröse Graphenmembranen (PG) deutlich senken, eine gleichmäßige Porenbildung auf großen Flächen ermöglichen und die Herstellung großflächiger PG-Membranen mit attraktiver Leistung erlauben. Ein skalierter Reaktor zur Synthese von Graphenfilmen im Metermaßstab konnte erfolgreich in Betrieb genommen werden. Zudem wurde ein großtechnischer Reaktor entwickelt, mit dem sich eine kontrollierte Oxidation des Graphens zur Erzeugung hochdichter Ångström-großer Poren für die CO_2-Abtrennung durchführen lässt. Mit diesem Reaktor können unter anderem Proben mit einer Fläche von bis zu 500 cm² hergestellt werden. Wir konnten zeigen, dass der Stofftransport des Oxidationsmittels – bislang kaum systematisch untersucht – eine entscheidende Rolle für die gleichmäßige Oxidation großflächiger Graphenfilme spielt. Für die Handhabung von Membranen mit zunehmender Größe (1, 10, 100, 500 cm²) wurden Querströmungsmodule entwickelt und validiert; auch das zuverlässige Abdichten der Membranen wurde erfolgreich umgesetzt. Die Bildung von Rissen beim Transfer des Graphens – ein Faktor, der bislang die Reproduzierbarkeit einschränkte – konnte durch ein neues Protokoll vollständig verhindert werden. Dieses Verfahren kommt ohne empfindliches Schwebenlassen oder manuelles Handling des Graphens aus und ermöglicht so die Herstellung leistungsstarker Graphenmembranen mit nahezu 100 % Erfolgsrate. Abschließend wurde der Membranprozess so optimiert, dass eine CO_2-Reinheit von 95 % bei einer Rückgewinnungsrate von 90 % erreicht wird. Unsere Herstellungsmethode hat die Reproduzierbarkeit und Erfolgsrate bei der Fertigung von Graphenmembranen deutlich verbessert. In Zusammenarbeit mit GAZNAT konnte zudem die Stabilität der Membranen bei der CO_2-Abtrennung aus Rauchgas nachgewiesen werden.

Résumé

La réalisation réussie de l'objectif zéro émission fixé par le Conseil fédéral suisse nécessite un développement rapide de technologies de capture du carbone à haute efficacité énergétique. Ce projet s'appuie sur la technologie innovante de membranes bidimensionnelles (2D) développée à l'EPFL, utilisant un film de graphène poreux d'épaisseur atomique comme couche sélective au CO_2. L'objectif est de porter cette technologie à l'échelle (membrane au mètre carré) et de démontrer la capture de 1 kg de CO_2 par jour.

À ce jour, plusieurs avancées ont permis de réduire considérablement le coût des membranes en graphène poreux (PG), d'assurer une formation homogène des pores sur de grandes surfaces, et de produire des membranes de grande taille avec des performances prometteuses. Nous avons mis en service un réacteur de synthèse à grande échelle capable de produire un film de graphène au mètre carré en un seul lot. Un second réacteur, également à grande échelle, a été développé avec succès pour oxyder de manière contrôlée le graphène, formant ainsi des pores de taille angström à haute densité pour la séparation du CO_2. Ce réacteur permet notamment de traiter des échantillons allant jusqu'à 500 cm². Nous avons démontré que le transfert de masse de l'oxydant, un paramètre encore peu étudié, joue un rôle déterminant dans l'obtention d'une oxydation uniforme sur des surfaces de graphène étendues. Des modules à écoulement transversal ont été développés et validés pour la manipulation de membranes de tailles croissantes (1, 10, 100, 500 cm²), accompagnés d'un scellement

efficace des membranes. La formation de fissures lors du transfert du graphène, facteur limitant la reproductibilité, a été éliminée grâce à un protocole innovant ne nécessitant ni flottaison ni manipulation délicate du graphène, permettant ainsi d'obtenir des membranes performantes avec un taux de réussite proche de 100 %. Enfin, le procédé membranaire a été optimisé pour atteindre une pureté en CO_2 de 95 % avec un taux de récupération de 90 %. Notre méthode de fabrication a considérablement amélioré la reproductibilité et le taux de succès dans la préparation des membranes en graphène. En collaboration avec GAZNAT, nous avons également démontré la stabilité de ces membranes pour la séparation du CO_2 dans des gaz de combustion.

Summary

A successful realization of the zero-emission target set by the Swiss Federal Council requires a rapid development of energy-efficient carbon capture technology. This project builds up on the EPFL's novel two-dimensional (2D) membrane technology using atom-thick, porous graphene film as CO_2-selective layer. The project aims to scale up the technology (meter-scale membrane) and demonstrate the capture of 1 kg CO_2/day.

So far, we introduce several interventions that significantly reduce PG membrane cost, allow uniform pore formation in a large area, and enable the preparation of large-area PG membranes with attractive performance. We have successfully commissioned a scaled-up reactor capable of synthesizing meter-scale graphene film in a single batch. We have also successfully developed a scaled-up reactor which can carry out controlled oxidation of graphene to form high-density Å-scale pores for CO_2 separation. In particular, this reactor can prepare samples that are up to 500 cm^2 in size. We show that mass transfer of the oxidant, which has not been systematically studied, plays a crucial role in achieving uniform oxidation of large-area graphene. We have developed and validated cross-flow modules for handling increasing size of graphene membranes (1, 10 cm^2, 100 cm^2, 500 cm^2) and have carried out successful sealing membranes. Crack formation during the transfer of graphene, which also limits reproducibility, is eliminated using a novel protocol that does not require delicate floating and handling of graphene, allowing the realization of a high-performance graphene membrane with near 100% success rate. Finally, we have optimized the membrane process to yield CO_2 purity of 95% with a recovery rate of 90%. Our method of fabrication has improved the reproducibility and success rate of preparing graphene membranes. In collaboration with GAZNAT, we have shown stability of graphene membranes in separating CO_2 from flue gas.

Contents

Abbreviations

2D: Two-dimensional

AC-HRTEM: Aberration-corrected high-resolution transmission electron microscopy

CHP: Combined heat and power

CFD: Computational fluid dynamics

CVD: Chemical vapor deposition

GPU: Gas permeation unit (1 GPU = 3.35×10^{-10} mol m^{-2} s^{-1} Pa^{-1})

IPCC: Intergovernmental panel on climate change

LAS: Laboratory of advanced separations

MRF: Mechanically reinforcing support film

NSLG: Nanoporous single-layer graphene

PES: Polyethersulfone

PG: Porous graphene

PTMSP: Poly(1-trimethylsilyl-1-propyne)

SLG: Single-layer graphene

SS: Stainless-steel

1 Introduction

1.1 Background information and current situation

The sixth assessment report by IPCC highlights the necessity to restrict the global temperature rise to within 1.5 ºC from the pre-industrial levels, which requires the reduction of CO_2 emissions from industrial point sources as well as atmosphere (negative emission).[1]

Among the point sources, power plants are the largest emitters with CO_2 concentration in flue gas amounting to 7-14%. There is also an intrinsic need to remove CO_2 from the raw biogas (with CO_2 concentration near 45%) which has started to play an important role in the Swiss gas grid. The captured CO_2 can be then converted into CH_4 using renewable electricity. This can be added to the gas grid leading to a reduction of overall carbon emission. Naturally, for the successful implementation of capture while realizing the energy needs of Switzerland, the development and deployment of energy- and cost-efficient capture technology is of paramount importance.

The need for energy-efficient technology comes from the high cost of capture from the currently commercially available technology, which is based on the absorption of CO_2 in an amine-based solvent. Here, the high cost (>CHF 50-110/tonCO_2) mainly arises from the requirement to regenerate liquid amines by thermal treatment.[2] High-performance-membrane-based capture processes can cut down the capture penalty because they do not rely on expensive thermal energy but instead on electrical energy (compression/vacuum) to create a concentration gradient across the membrane. The current membrane-based capture technology is based on dense polymeric films as the selective layer. The state-of-the-art polymeric films have shown promising CO_2/N_2 performance.[3] However, there is an opportunity (i) to significantly improve separation performance, especially the CO_2 permeance which affects the needed membrane area and, therefore, the capital cost, and (ii) to improve the operational life of the membranes. Thermally and chemically stable nanoporous inorganic material-based selective layer has an intrinsic advantage of high CO_2 permeance and improved thermal and chemical stability.

LAS at EPFL has developed an extremely thin nanoporous inorganic film composed of an atom-thick porous graphene layer for high-performance carbon capture. We have demonstrated high carbon capture performance with CO_2 permeance approaching 10000 GPU and CO_2/N_2 selectivity above 20. The CO_2 permeance, which determines the needed membrane area, is an order of magnitude better than that of commercial membranes. Technoeconomic analysis of these membranes indicates significant energy and cost savings for carbon capture.

1.2 Purpose of the project

Our techno-economic analysis indicates that a double-stage membrane module fitted with high-performance graphene membranes with only a small membrane area of 0.04 m^2 is sufficient for capturing 1 kgCO_2/day (our target rate) in an energy-efficient manner.[4] Given the high potential of this technology in addressing the important issue of global warming, its further scale-up and demonstration are attractive. Therefore, the project will seek to scale up the production of nanoporous graphene films, membrane elements, and membrane modules. Subsequently, the project will build a two-stage membrane process to capture CO_2 from flue gas and biogas with the help of our industrial collaborators.

1.3 Objectives

This project aims to scale up porous graphene films hosting Å-scale pores for gas separation to a large area (50 cm^2 scale for a single coupon). The project then intends to develop a membrane element and

module using graphene film as the selective layer. The membrane will be implemented in a two-stage membrane process to capture CO_2 at the rate of 1 kg/day from a simulated CO_2/N_2 gas mixture.

Overall, by testing high-performance membranes, we aim to validate the analysis from our techno-economic analysis (Table 1).

Table 1. Techno-economic analysis of carbon capture from different feed conditions.

Feed Condition	Recovery	Purity	Specific Energy Demand ($GJ/ton CO_2$)	Capture Cost ($/ton CO_2)	Membrane Lifespan (year)
Flue gas (12% CO_2)	90% CO_2	90% CO_2	1.5	41	5
Biogas (45% CO_2)	96% CO_2, 91% CH_4	90% CO_2, 96% CH_4	0.7	38	5

Our specific objectives are:

1. Scale-up production of high-performance graphene membranes (target area 0.1 m^2) using intrinsically scalable fabrication methods that are capable of yielding m^2 graphene membranes in a single synthesis batch.
2. Develop compact plate and frame membrane modules that have a low volume footprint and high packing density (100-300 m^2/m^3) but low-pressure drop while avoiding concentration polarization.
3. Build membrane skids consisting of a double-stage membrane process with recycle, and demonstrate its efficacy for capturing 1 kg CO_2 from a gas mixture representing flue gas from a waste incinerator with recovery of 90% and purity of 95%.
4. Demonstrate membrane stability by continuously online monitoring the performance data.

2 Description of facility

2.1 Membrane production

As a part of the project, we have built a dedicated scale-up laboratory to produce high-quality graphene membranes in a clean environment. The equipment includes an ISO 5 cleanroom (Figure 1), a homemade reactor to produce porous graphene at meter-scale (Figure 2 and Figure 3), a scaled-up oxidation reactor to synthesize porous graphene (Figure 4), and a large-area spin-coater (Figure 5) to deposit a thin protective and mechanically-reinforcing polymeric film on graphene.

The cleanroom (ABN Cleanroom Technology, ABNCR-22 580, ISO 5) has an air exchange rate of 70 times per hour and less than 1000 1-µm-sized particles per cubic meter. It covers an area of 4 m × 3.5 m. The cleanroom is designed in a way such that all gas connections reach inside the cleanroom without disrupting the cleanroom module extensively. There is also air conditioning provided in the side clean room to ensure that the temperature of this enclosure does not go up when ovens heat to high temperatures.

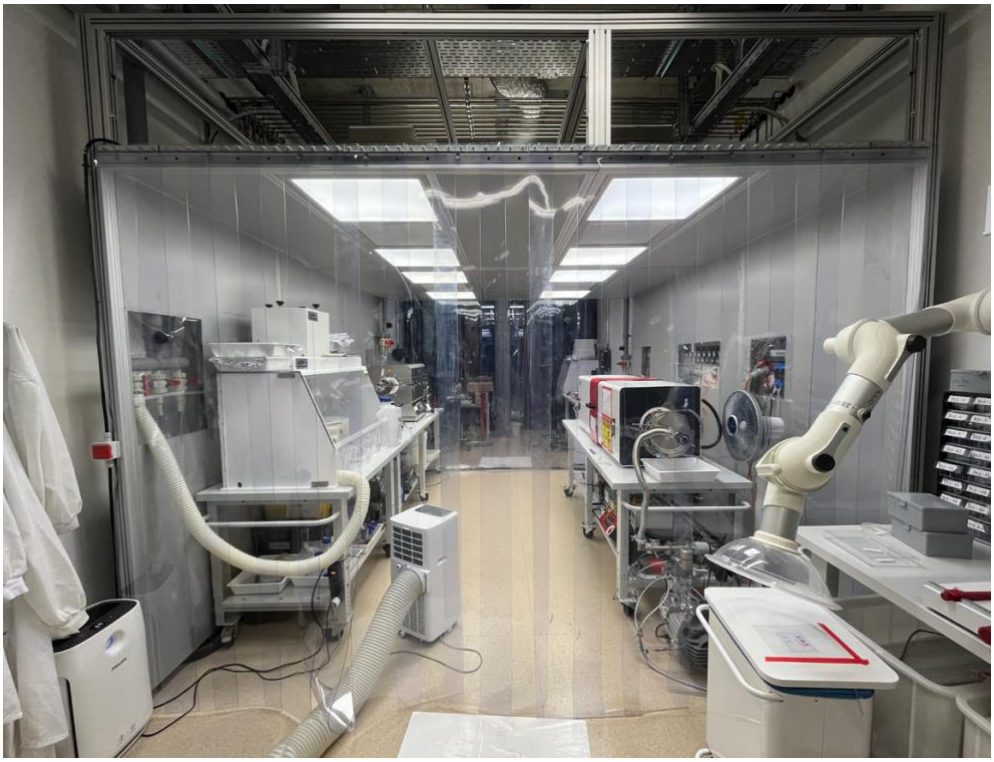

Figure 1. The membrane scale-up laboratory at EPFL.

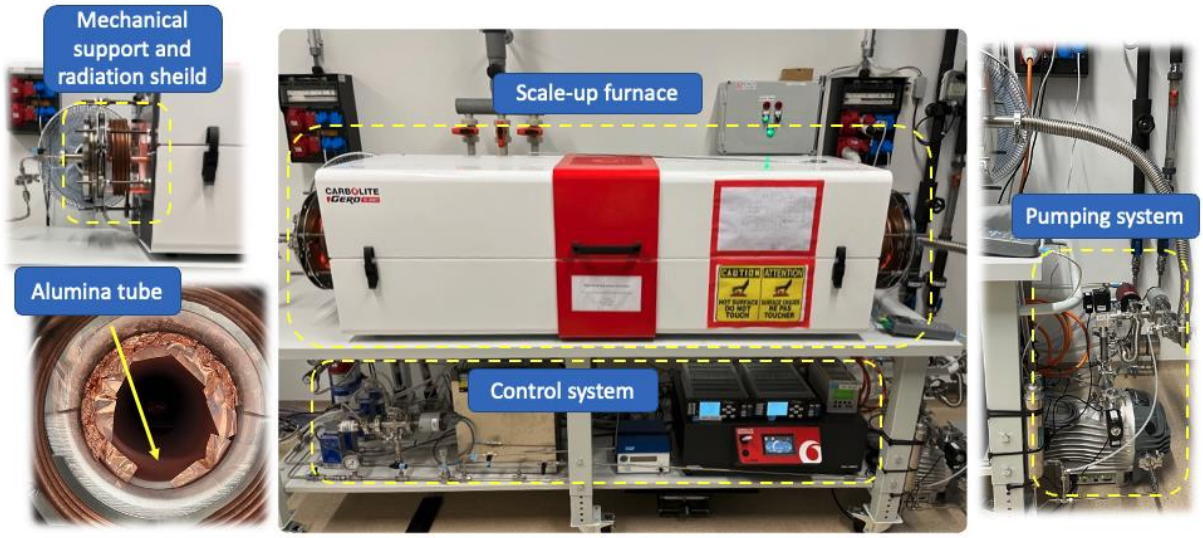

Figure 2. Large-scale CVD furnace for graphene synthesis.

The large-scale CVD furnace is custom-made in the laboratory. It is composed of a heating furnace (Carbolite, 1200 ℃ Split Tube Furnace, TS3 12/200/1200, with a controller, see Figure 2) which has a 1.2 m uniform heating zone up to 1200 ℃ and is equipped with a quartz tube with an outer diameter of 20 cm. Inside the quartz tube, an alumina tube (Zibo Highlion New Material Co., Ltd, 1.5 m long, outer diameter of 18 cm, inner diameter of 16 cm) is placed to reduce the contamination from the quartz tube.

This is because, during the heating of Cu foil above 600 ºC, the reaction between Cu vapor and quartz produces SiO_x particles and contaminates the Cu surface.

It can be used to produce graphene coupons with a width of 12 cm and a length of 1 m. The furnace is equipped with different systems to run a synthesis. We customized a stainless-steel mechanical support to withstand the compression force from the metal flanges during pumping. We realized that it is extremely crucial to balance the mechanical force on the quartz tube when the vacuum is applied. This is where the mechanical support is crucial (shown on the left side of Figure 2). We also added a customized copper radiation shield near the edge of the heating zone inside the quartz tube to reduce the flange temperature during synthesis. The system is pumped through a scroll vacuum pump (Plasmadiam, nXDS 10i), and the pressure is monitored by several pressure transducers (MKS, Vacuum Pressure Transducer, 1000 Torr, and 1 Torr). A gas regulating valve (Pfeiffer, RVC 300) is integrated to regulate the system pressure during synthesis. The synthesis can be fully automated by creating LabView programs to interact between these devices and a laboratory PC, and the software interface is shown in Figure 3.

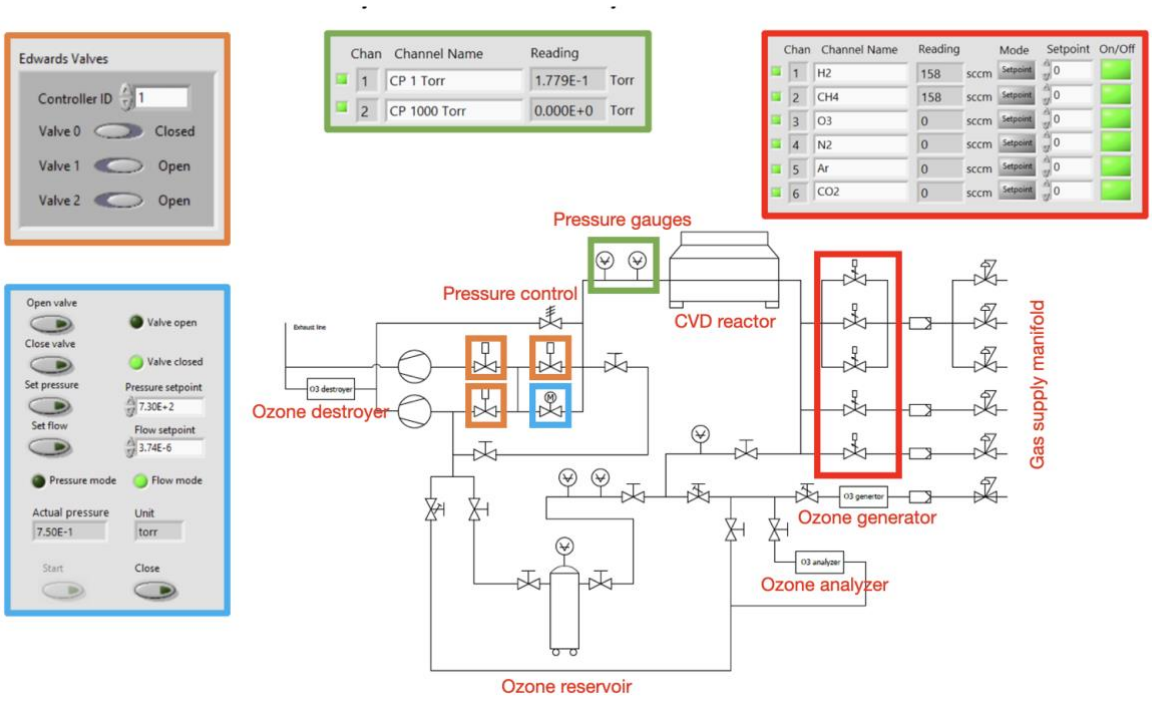

Figure 3. Process flow diagram for the large-scale CVD reactor for producing nanoporous graphene.

The graphene oxidation reactor, responsible for creating pores in graphene, is equipped with a furnace (Nabertherm, Split Tube Furnace, RSH, Figure 4) hosting a 12 cm diameter quartz tube. The reactor can be heated to a temperature of 1100 ºC, and its pressure can be controlled by a vacuum pump. The pressure is monitored by a Baratron absolute manometer (MKS). The reactor can house graphene coupons with a width of 11 cm and a length of 50 cm. The reactor is fed with an ozone supply via an ozone generator (Absolute Ozone, Atlas 60) with a concentration of 8-10% ozone in oxygen and a flow rate of up to 2 l/min at atmospheric pressure. It is also fed with argon and hydrogen, which is used to clean the graphene surface from contamination. The laboratory is equipped with ozone sensors and an automated ozone flow cutoff system in case of a leak of ozone.

Figure 4. Large-scale tube furnace for ozone functionalization on graphene.

The laboratory is also equipped with a large area spin coater (Laurell Technologies Corporation, WS-650Hz-15NPPB) capable of coating thin polymeric film for large substrates (up to 30 cm diameter coupons, Figure 5). For meter-scale graphene membranes, this is a sufficient and convenient route to reliably coat a thin polymeric film. The spin coater is housed in a ventilated hood which allows one to use organic solvent-based coating suspension.

Figure 5. Large-area spin coater hosted inside a ventilated hood.

A dedicated space outside the Engerypolis campus was built for testing and demonstrating carbon capture from a gas mixture using porous graphene membranes (Figure 6). Pure CO_2, N_2, and O_2 gases can be supplied from gas cylinders to mimic the composition of the flue gas. An automated testing system has been built with remote monitoring functionality to generate continuous data to evaluate the long-term graphene membrane stability (Figure 60). Moreover, real flue gas with SO_x/NO_x contaminants will be used to test the membrane stability under real flue gas conditions.

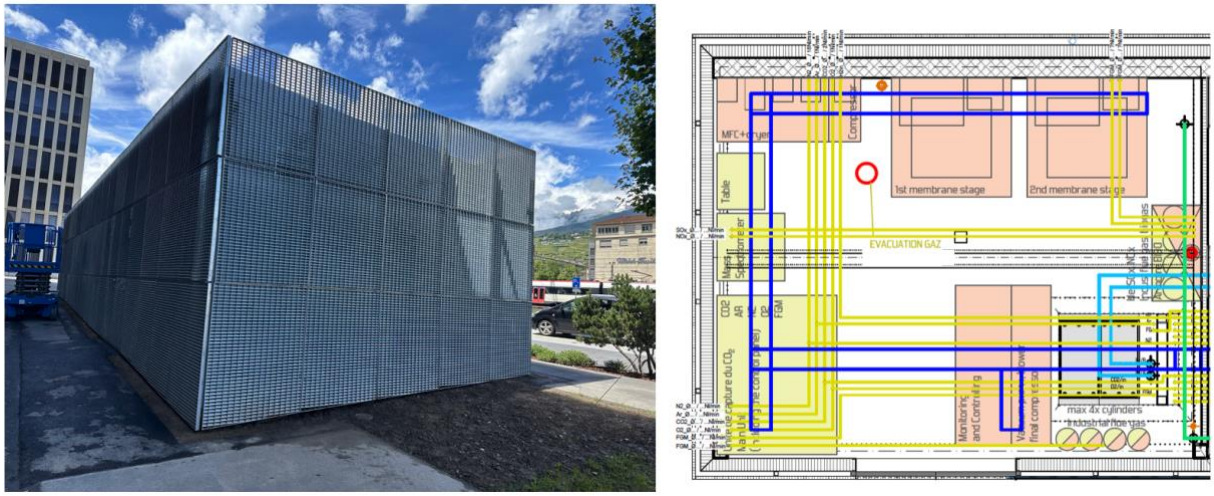

Figure 6. Dedicated space in Energypolis campus (Sion) for the demonstration of graphene membrane-based carbon capture

2.2 Membrane setup

In this section, we describe the graphene membrane and its characterization. The graphene membrane described here refers to porous graphene film with a selective layer thickness of just one atom. Graphene is an allotrope of carbon formed of a single layer of graphite where carbon atoms are arranged in sp^2-hybridization. As a result, pores in graphene constitute the thinnest possible permselective layer. The single-atom thickness of the pore translates into an extremely small molecular diffusion path length and leads to a high permeance of gas molecules. If small pores, similar to the size of gas molecules, are incorporated in graphene, the separation of gas molecules takes place based on the relative rate of diffusion of gas molecules from the pore (Figure 7). This rate of diffusion depends on the energy barrier of the molecule to cross the pore, which, in turn, depends on the relative size difference of gas molecules with respect to the nanopores, a concept termed molecular sieving. In the separation of flue gas, two major components are CO_2 and N_2. Luckily, CO_2 is smaller than N_2 (kinetic diameters of 0.33 and 0.364 nm, respectively), which allows one to target their separation from graphene pores. Another pathway that affords selectivity to CO_2 is competitive adsorption of CO_2 vs N_2 on graphene pores. This is especially manifested when the graphene pores are functionalized (e.g., with an O or N functional group). In our case, since pores are created by oxidation, the pores are decorated with O functional groups (epoxy, ether, semiquinone).

The advantage of graphene membranes as against commercial membranes such as those made of polymer comes from the fact that graphene pores allow rapid transport of gas molecules. As a result, graphene membrane yields a higher CO_2 permeance compared to polymeric membranes, which is advantageous to cut the needed membrane area and, therefore, the cost of the capture. This also becomes extremely useful for the compaction of the membrane process, especially when space for installation comes at a premium (offshore facilities, transportation sector, etc.).

Porous graphene has another advantage. It has high chemical, thermal, and mechanical robustness. Therefore, one can expect a much longer lifetime of graphene membranes, although this needs to be validated. In our experiments, we have observed stable performance for a long period extending to more than a year. This is because of the inorganic lattice of graphene. Based on this, we expect a membrane lifetime of at least five years.

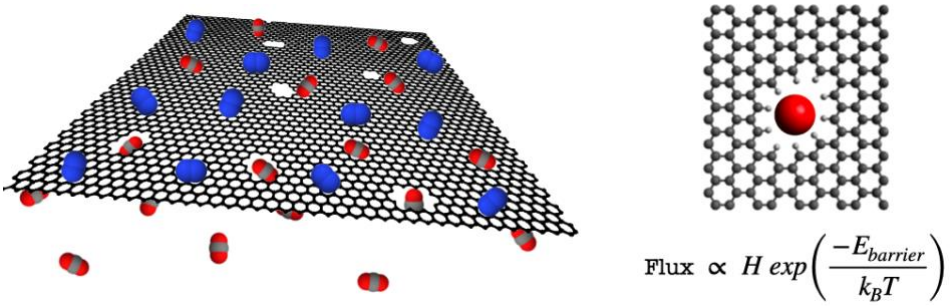

Figure 7. Schematic showing separation of CO_2 from N_2 from porous graphene film (left). The flux of gas across a graphene pore is determined by the relative difference between the size of the pore and that of the gas molecule. The relative size difference determines the energy barrier for the molecule to cross the pore and hence also determines the size-based gas pair selectivity.

The prepared membrane is first assembled in a membrane module (see next section for the preparation technique), and the module is further inserted in a permeation measurement setup to validate the gas separation property. Figure 8a shows a schematic illustration of the permeation setup on a laboratory scale, and Figure 8b shows the example of different segments. Different feed gases travel across the surface of the membrane. Part of the feed gas will go through the membrane, and the rest will be in the retentate. The membrane enables a selective permeation rate for CO_2. As illustrated by a cartoon in Figure 8c, our membrane has a higher CO_2 transport rate than N_2, which realizes an enrichment of CO_2 gas on the permeate side.

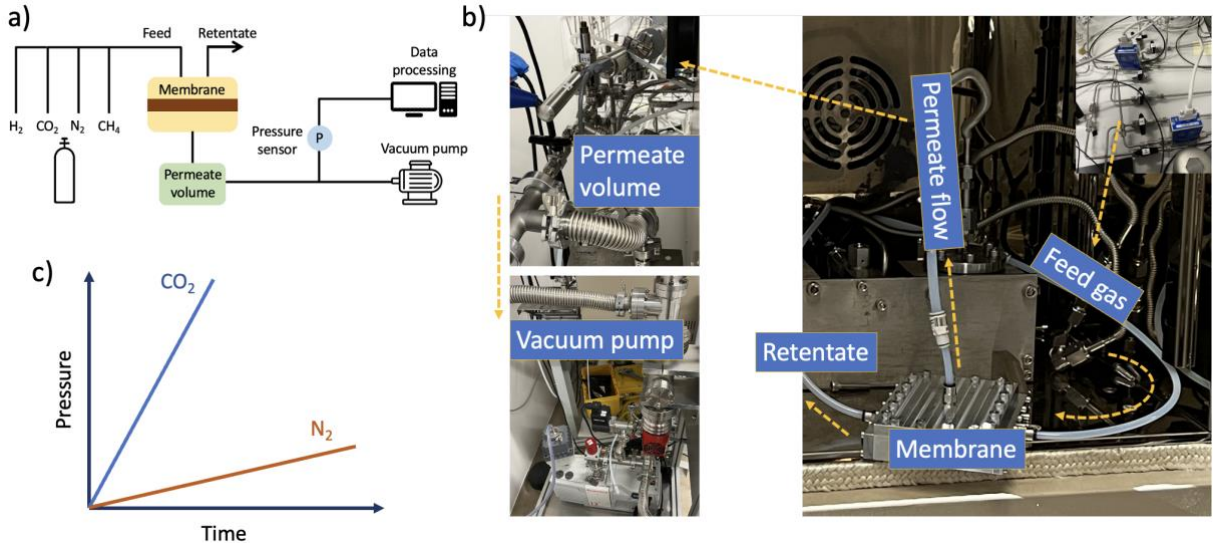

Figure 8. A). Schematic illustration of the membrane separation process on a laboratory scale. B). Examples of different segments of the membrane permeation setup. C). Schematic illustration of membrane permeation results showing that CO_2 gas is passing through the membrane faster than N_2.

We have also developed a membrane skid for industrial-scale testing to reach a high CO_2 recovery and purity (Figure 9 and Figure 10). Briefly, this will direct testing of flue gas separation by feeding simulated flue gas as well as real flue gas to the membrane consisting of 10-12% CO_2. EPFL in collaboration with HES-SO has built a satellite site on the EPFL Valais campus. The membrane skid is being commissioned at this demonstration site. A detailed process flow diagram of using a two-staged membrane module for carbon capture is shown in Figure 9.

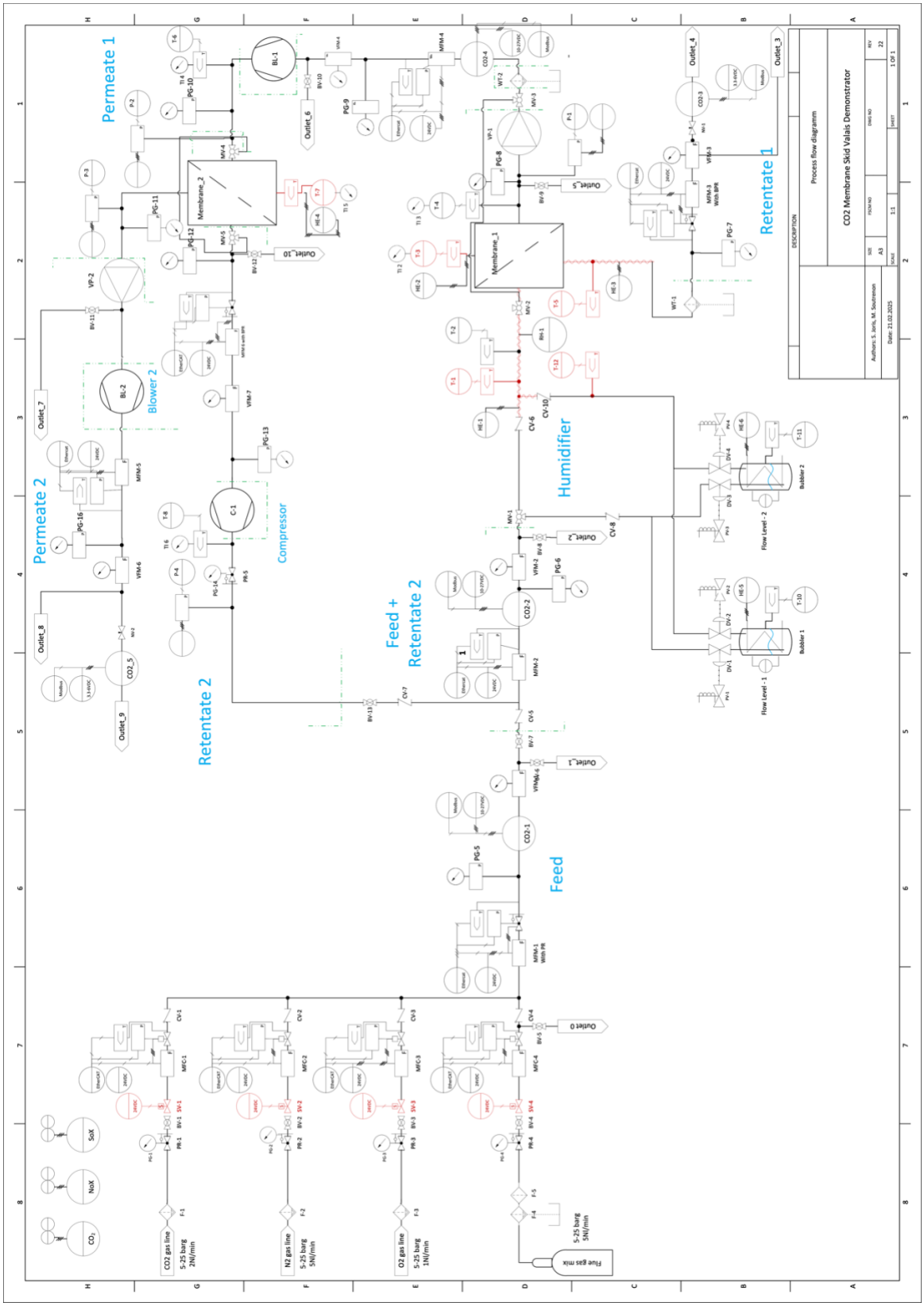

Figure 9: Process flow diagram of the two-staged membrane skid (see pictures of the skid in Figure 10).

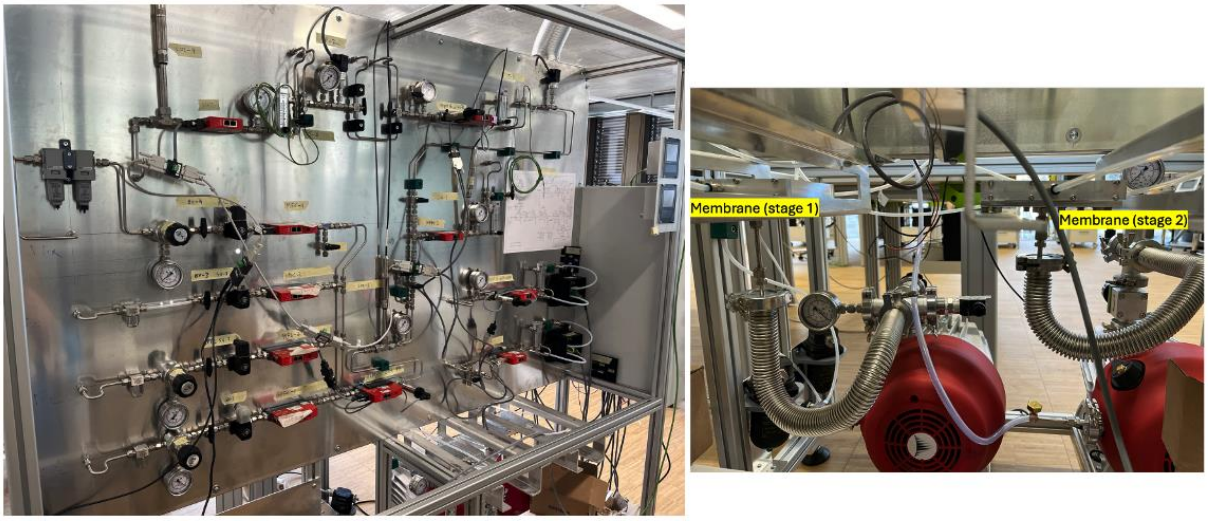

Figure 10. The two-staged membrane skid (left). Right: The two membrane modules are highlighted on the right.

Before the start of this project, graphene membranes that demonstrated successful separation of CO_2 from N_2 were still on a scale of a millimeter or a centimeter. The success rate in the preparation of these membranes was low (e.g., 20%, which means that only one in five membranes would have a good performance). With this project, we have successfully developed a membrane fabrication route to produce centimeter-scale graphene membranes with a near 100% success rate. We further extend this method to prepare membranes with an area of 250 cm^2. We have developed a highly scalable oxidation approach, different than the one used for the proof-of-concept (which was challenging to scale-up). We demonstrate that CO_2 permeance of 2000-3000 GPU, with a CO_2/N_2 selectivity of 17-25, can be achieved by this method. Further optimization is foreseen to further improve the permeance to 10000 GPU and selectivity to 50. This will help to improve the CO_2 separation efficiency and cut down the capture penalty.

3 Procedures and methodology

3.1 Project procedure

The fulfillment of this project can be described in the following procedures:

1. Building a cleanroom facility-based laboratory that has a satisfactory contamination level from the air for the production and processing of clean graphene membranes.
2. Designing and assembling experiment setups for low-pressure CVD synthesis.
3. Designing and assembling experiment setups for graphene oxidation using ozone.
4. Optimizing the experimental parameters to synthesize graphene with high quality and high porosity.
5. Optimizing and scaling up the membrane module for reproducible membrane fabrication and reliable mixture gas separation.
6. Constructing membrane separation units in the lab to understand performance.

7. Development of process model and carrying out technoeconomic analysis to understand the optimal configuration for membrane process (pressure ratio, area, recycle in the two-stage stage membrane, etc.).
8. Development of a membrane process to validate the performance of our membrane process.

To realize high-performance graphene membranes, our strategy was the following:

1. Studying the key factors that affect the quality of graphene synthesized by the CVD approach. This includes surface quality of Cu (roughness, contamination), Cu annealing conditions, CVD synthesis temperature, synthesis pressure, and precursor concentration.
2. Studying the influence of different ozone gas reaction parameters on the porosity and the pore size distribution of graphene by directly analyzing the membrane performance. Here, CO_2 permeance is an indicator of porosity in graphene, whereas CO_2/N_2 selectivity is an indicator of efficacy in creating a narrow pore size distribution. Key parameters studied for this were reactor geometry (diameter), temperature uniformity, ozone flow rate and velocity, reaction temperature, time, and Cu surface roughness during the reaction. The latter was optimized by annealing the porous graphene in a hydrogen atmosphere at various temperatures to get a smooth Cu surface.
3. Designing the membrane mechanical reinforcement strategy for defect-free membrane fabrication, as well as the membrane module geometry for efficient single component or mixture gas separation.

3.2 Synthesis of high-quality, large-area single-layer graphene

The procedure for the synthesis of high-quality single-layer graphene in the scale-up CVD furnace consists of several steps. This starts with cleaning the surface of as-received Cu foil (Roth, 100 μm thick) by acid treatment. Briefly, Cu foil is cut into desired sizes and undergoes an acid treatment to remove the surface coatings or impurities, which can be preserved after graphene synthesis. The acid treatment is done by first immersing Cu foil into 4 wt% nitric acid for 10 min and then washing it in deionized water 4 times. The resulting Cu coupon is then inserted in the CVD reactor for synthesis.

In the CVD reactor, the cleaning of organic contaminants takes place by exposing Cu to CO_2. This is followed by H_2 annealing to reduce any native oxide groups on Cu, graphene synthesis by CVD, and finally, cooling (Figure 11). CO_2 cleaning is done below 1020 ℃ under ambient pressure, after which the atmosphere is changed to H_2/Ar for annealing of Cu. The annealing procedure is optimized close to the melting point of Cu, followed by a stepwise cooling to the CVD growth temperature (1020 ºC). The synthesis is done at 190 mTorr maintained by flowing 3 and 9 sccm of H_2 and CH_4, respectively. After 30 min of synthesis, the furnace is cooled down naturally.

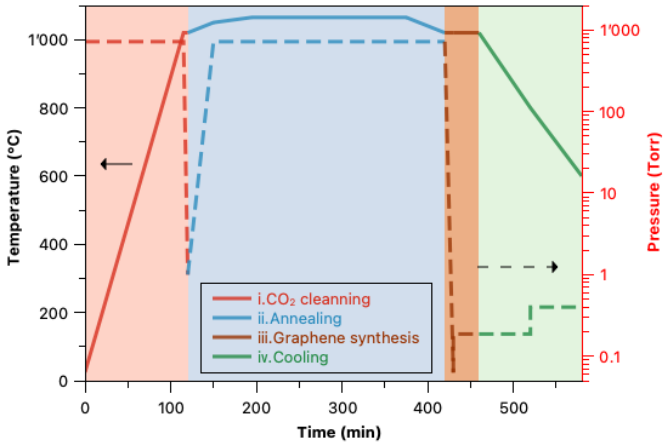

Figure 11. Large-scale CVD protocol for graphene synthesis.

3.3 Pore opening in graphene by ozone treatment

The oxidation of graphene was systematically optimized based on an improved fundamental understanding of graphene oxidation in O_3 based on recent studies from our group (see publication section). The experiment setup illustration of ozone oxidation is shown in Figure 12a, and the process of oxidation consists of four consecutive steps (Figure 12b):

1. Graphene is first cleaned in a reductive atmosphere at 600 ℃ to remove the surface contamination on graphene as well as reduce any oxidation on the substrate (Cu).
2. Graphene is then soaked in ozone flow after cooling the sample to the oxidation temperature (50-80 ℃). The sample is typically exposed for a period of 1 h to 6 h, during which temperature is maintained or is cooled down to room temperature (see results sections). During this process, oxygen clusters on the graphene lattice are formed. There are a few parameters to tune for maximizing the cluster density, including ozone reaction temperature and time, and gas velocity across the sample. It should be noted that ozone supply is achieved from the ozone generator which requires 30 min of operation to obtain a steady state. Therefore, ozone flow is initiated at least 30 minutes before ozone is injected in the reactor. In this time gap, generated ozone is similarly purged out to the evacuation system after destroying ozone with an ozone destroyer.
3. The above step generates oxygen clusters on graphene which are typically 2-3 nm in size. Pores are opened by gasification of these clusters by heating to 150-200 ºC in an argon atmosphere.
4. Cu surface is usually oxidized and becomes rough during the oxidation step (Figure 12c, d). Our efforts to prepare membranes using as-oxidized graphene failed likely because it is challenging to transfer graphene from rough Cu foil. In order to get a better membrane, the Cu surface is reduced. For this oxidized graphene film resting on Cu foil is finally reduced under H_2/Ar at 500-600 ℃.

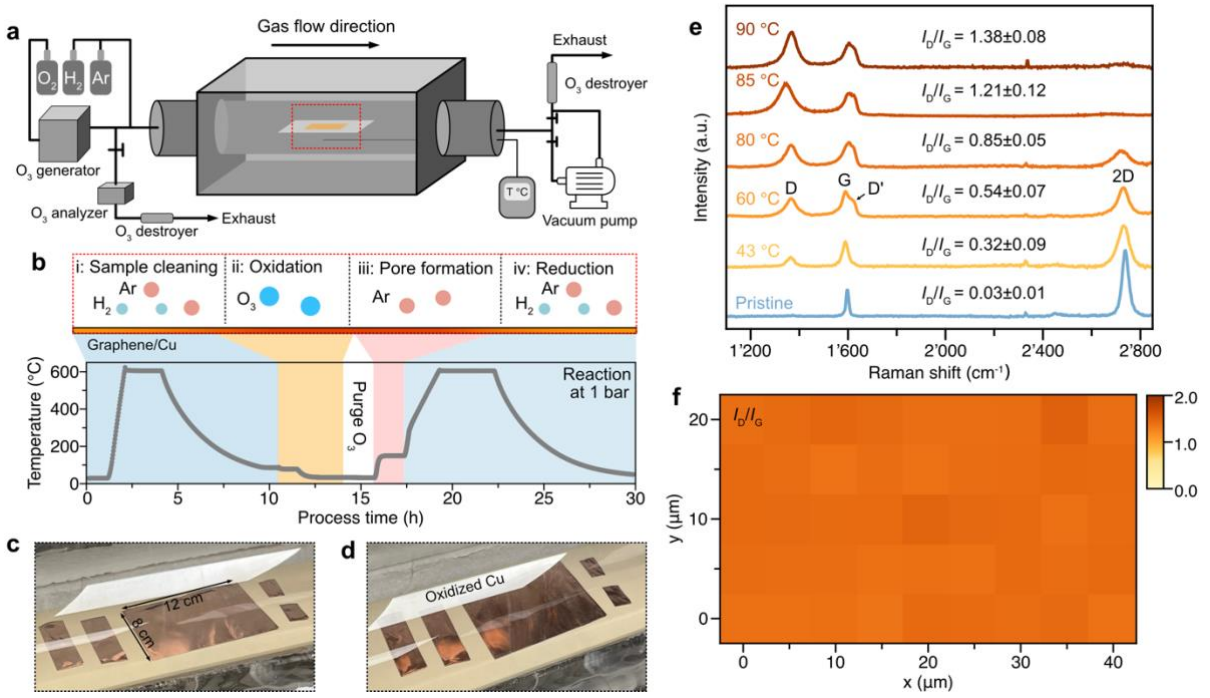

Figure 12. Scaled-up reactor for pore incorporation in graphene. a, Schematic illustration of the ozone functionalization setup. b, Oxidation schemes with corresponding temperature profiles used in the process. c,d, Photos of graphene resting on Cu before (c) and after oxidation (d) where color change of oxidized Cu can be visualized. e, Raman spectra of graphene under various temperatures for oxidation. The spectra have been normalized to the G band intensity. f, Raman mapping of D/G peak intensity ratio of graphene oxidized at 90 ℃ across an area of 20 × 40 μm^2.

After ozone oxidation, Raman spectroscopy is used to characterize graphene. An example in Figure 12e clearly shows that defects are introduced on the graphene lattice because *D* peak is introduced. Figure 12f shows a uniform oxidation achieved by our approach. CO_2 permeance (measured in gas permeation units or GPU, 1 GPU = 3.35 x 10^{-10} mol m^{-2} s^{-1} Pa^{-1}) is dependent on the extent of oxidation which determines pore density and size. The more the sample is oxidized, the higher the membrane permeance will be. But at the same time, there is also a trade-off between membrane permeance and selectivity. The loss in selectivity at higher pore density is because neighboring pores may coalesce to form larger pores, which would not be selective. The process is then optimized to obtain overall high performance.

3.4 Membrane fabrication

The MRF approach has been reported to address the crack formation in graphene during its transfer. While centimeter-scale membranes have been reported, the success rate has been low from stress generated in the film during wet-chemical etching of the film where the film is floated. To address this issue, we developed a facile transfer strategy involving a novel membrane module architecture (Figure 13a, b). This involved coating an MRF (PTMSP) on PG with a target thickness close to 1 μm (Figure 13c). The resulting Cu/PG/MRF was placed on a porous membrane support (PES), ~0.2 μm pores, Figure 13d) resting on a macroporous stainless steel (SS, Figure 13e) mesh. Step-by-step assembly of the module with a stacking order of Cu/PG/MRF/PES/SS mesh is illustrated in Figure 13f. The module was sealed by two rubber gaskets (Figure 13b) and was compressed by two cover plates (Figure 13f, panels i and ii).

The stacking order, Cu/PG/MRF/PES/SS mesh, exposes Cu foil on one side of the module, allowing one to etch and remove Cu directly from the assembled module. This effectively eliminated the need to float graphene. After sealing the module, the exposed Cu was placed in contact with a cell hosting a Cu etchant (1 M $FeCl_3$, Figure 13f, panel iii). During etching, PG reinforced by MRF was secured in the module.

Optical microscope (Figure 13g) and SEM images (Figure 13h, i) of the graphene surface exposed after removing Cu reveal the absence of any visible cracks. The white particles observed in Figure 13h are residues from the etching of Cu foil. The reproducibility of this transfer strategy was probed by cutting a ~8 × 12 cm^2 graphene coupon (Figure 13j) into 24 pieces of 2 × 2 cm^2 coupons (Figure 13k) and fabricating membranes from each coupon (Figure 13l).

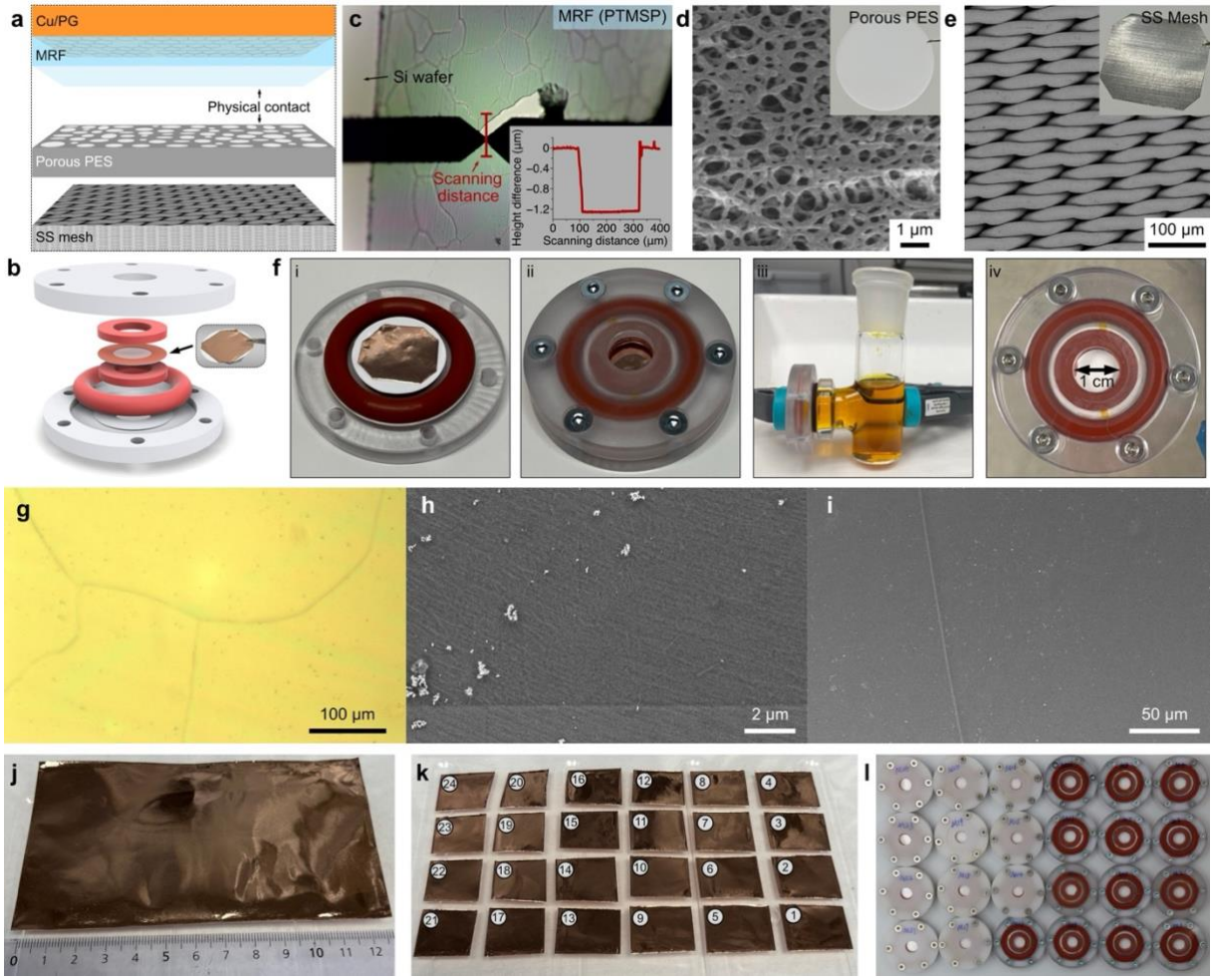

Figure 13. Crack-free direct transfer of graphene inside the membrane module. a,b, Schematic illustration of graphene transfer strategy (a), and the architecture of the membrane module (b). c, Optical microscope image of the MRF transferred on a Si/SiO_2 wafer. The inset shows the film thickness characterization. d,e, SEM images of commercial polyethersulfone (PES) support (d) and stainless steel (SS) mesh (e). The insets are pictures of the two supports. f, Pictures of stacked membrane assembly hosting Cu/PG/MRF/PES/SS mesh (panels i and ii), etching setup for Cu (panel iii), and as-prepared graphene membrane module after etching Cu foil (panel iv). g-i, Optical (g), and SEM (h, i) images of graphene surface after removal of Cu. j-k, A ~8 × 12 cm^2 graphene coupon (j) is cut into 24, 2 × 2 cm^2 small coupons (k). l, All 24 coupons in panel (j) lead to successful 1-cm-scale membranes. Half of the membrane modules were assembled with transparent cover plates to reveal the sealing.

The simple design of this module allowed the upscaling of the membrane element. However, the circular disk design of the above module limits the ability to achieve the practical cross-flow configuration. Therefore, larger decimeter-scale modules were designed by including cross-flow permeation channels (Figure 14). The membrane stacking order and Cu etching strategy were identical (Figure 14a). The module consisted of a symmetrical body frame and two identical cover plates to pack two 5-cm^2-sized membrane elements in a single module to increase the packing density. A cross-flow channel was created using slits on the side of the module (Figure 14b). Cu foil in the assembled module could be removed by flowing the etchant through the cross-flow slits (Figure 14c). This exposed graphene and generated a feed channel for gas permeation experiments. The cover plate on both sides had a central opening serving as a permeate window. This module could be further scaled into a larger one capable of hosting two 5 × 10 cm^2 membrane elements (Figure 14d).

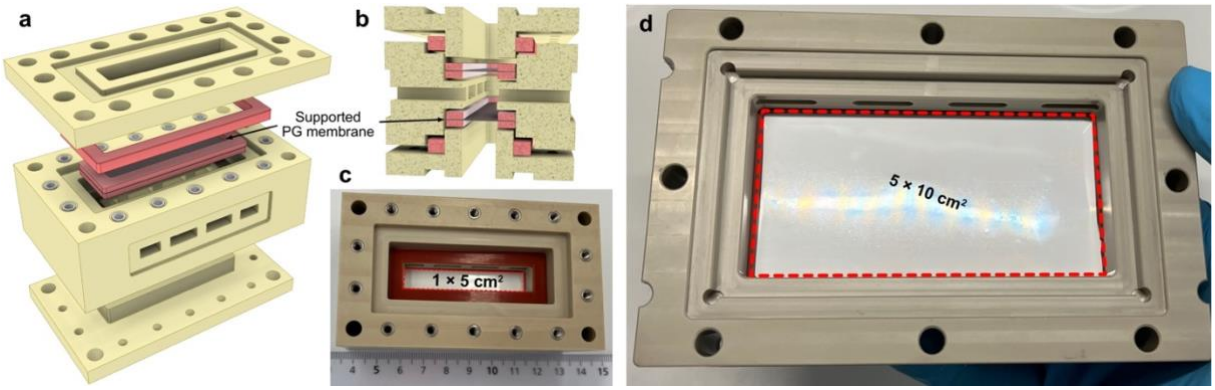

Figure 14. Graphene membranes prepared in large-area cross-flow modules. a,b, Three-dimensional model of the upgraded membrane module architecture (a), and the corresponding cross-section view showing the cross-flow slits (b). c,d, Photos of successfully prepared 1 × 5 cm^2 (c) and 5 × 10 cm^2 graphene membranes (d).

3.5 Permeation test

The robustness of the graphene membrane is validated by permeation measurements using a constant-volume variable-pressure setup (Figure 15). Very briefly, membrane is exposed to feed gas (single component). The permeate collects in a fixed volume leading to rise in the pressure of the permeate. This is then used to calculate the permeance of the membrane as a function of feed gas type and membrane temperature. For evaluating mixture gas, the permeate gas is sent to gas chromatograph where gas composition analysis is carried out.

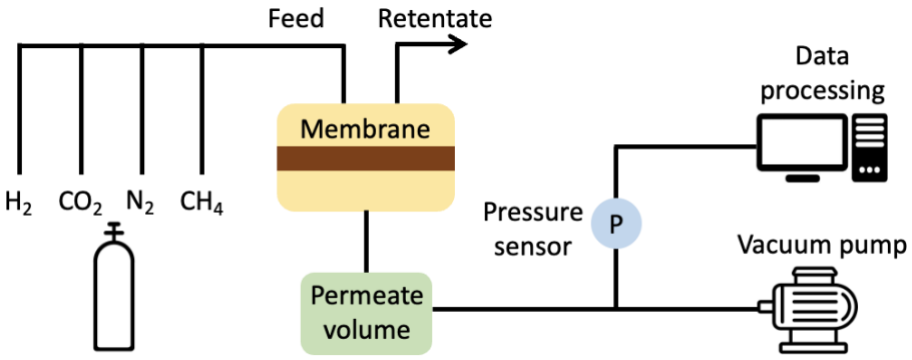

Figure 15. Schematic illustration of the membrane permeation test setup.

4 Activities and results

4.1 Summary of activities in the previous report

The activity in the previous report period focused on preparing a low-cost Cu foil for graphene synthesis, assembling a large-scale CVD reactor, developing transfer protocols for preparing crack-free membranes (1 cm^2) packed in a novel membrane module, and improving process configuration to achieve the target recovery and purity.

For the Cu foil, the activity focused on ensuring a highly smooth and contamination-free surface of Cu to synthesize graphene to achieve parity results with higher cost counterparts. For this, foil preparation techniques were optimized.

For the CVD reactor, the process focused on developing protocols that minimize contamination in graphene during graphene, allowing the synthesis of high-quality polycrystalline film and allowing operation in a safe and controllable manner, especially limiting the heating of end connections for CVD to 100ºC. For this, novel radiation shields were designed, and water cooling was implemented (Figure 2).

The module was designed to reduce the nonideal effects of concentration polarization and pressure drop. For this, flow channel width was optimized.

Technoeconomic calculations focused on reducing the capture penalty for achieving target purity and recovery.

Detailed activities and corresponding results, focusing on last one year of development are discussed below.

4.2 Preparation of low-cost Cu foil

Our proof-of-principle results on high-performance graphene membranes were obtained on expensive Cu foil with a cost over 8000 CHF/m^2. To decrease this cost, we developed lower purity Cu foil alternates (Table 2).

Table 2. Comparison of the Cu substrate used in this work and the market.

Supplier	Catalog No.	Purity	Thickness (µm)	Price (USD/m^2)*	Demonstration of high-quality graphene	To make gas-sieving membranes
Nilaco	CU-113221	99.99+%	25	16735	Yes	No
	CU-113263	99.9%	50	35	Yes	No
Strem	STR93-2994	99.9%	50	9100	Yes	Yes
Sigma-Aldrich	349208	99.98%	25	2473	Yes	No
Goodfellow	1000070388	99.9%	50	1598	Yes	No

Alfa Aesar	13380.cv	99.9%	127	740	Yes	Yes
	46986.RH	99.8%	25	214	Yes	Yes
Basic Copper	cu-3mil-6in-4ft cu-3mil-bulk-roll	99.9%	76	156 39	Yes	No
Roth	8540.2	99.9%	100	100	Yes	This work
MTI KJ group	BCCF-25u-B	99.8%	25	29	Yes	No
Kunshan Luzhifa Electronic Technology Co., Ltd.		99.97%	50	10	Yes	No
Alibaba	C1100	99.9%	100	10	Yes	This work

*Note: the price is sensitive to market dynamics.

100 µm-thick Cu foil from Carl Roth® with a cost of 87 CHF/m^2 was chosen because it fits the cost projected in the technoeconomic analysis. The cost of the Cu foil could be further cut down to 10 USD/m^2 (see Table 2) where high-quality graphene could also be synthesized. We chose a thicker foil because it is easier to handle (lesser degree of bending and folding which is good for graphene transfer). The Cu foil is processed to reduce surface roughness and contamination (Figure 16, detailed description can be made available on request).

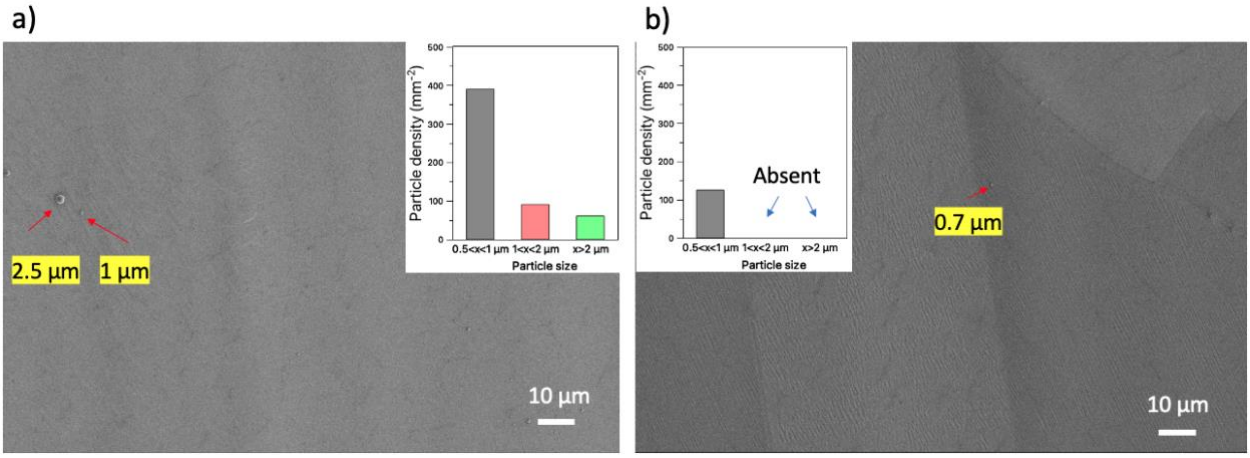

Figure 16. SEM image of graphene surface synthesized on a) as-received Cu and b) treated Cu. The inset is the contamination particle density after graphene synthesis.

4.3 High-quality, large area graphene synthesis:

By our above-mentioned CVD synthesis method, large-area graphene coupons (11 x 26 cm) could be successfully synthesized (Figure 17). The high quality of graphene is evident by the Raman spectroscopy. The spectrum shows a negligible defect peak (*D* peak), and a map of peak intensity ratio (*D*/*G*) shows that the quality of graphene is uniform (Figure 18). Figure 19 shows that the graphene has similar quality throughout the entire reactor.

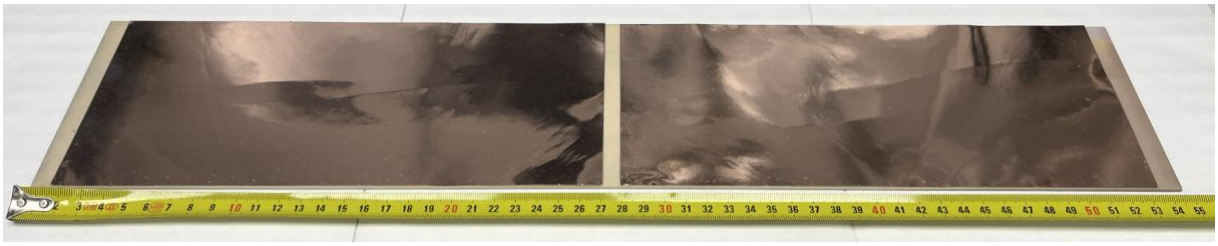

Figure 17. Large coupons of graphene synthesized in the large-scale CVD furnace.

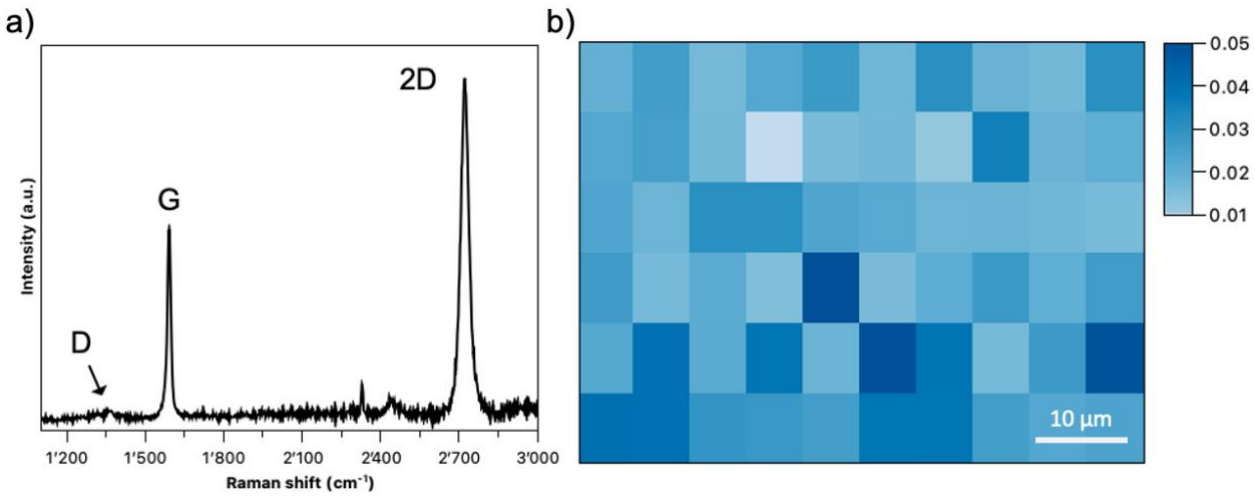

Figure 18. a) Raman spectrum of SLG, and b) the color map of I_D/I_G ratio on a 60 x 40 µm^2 area.

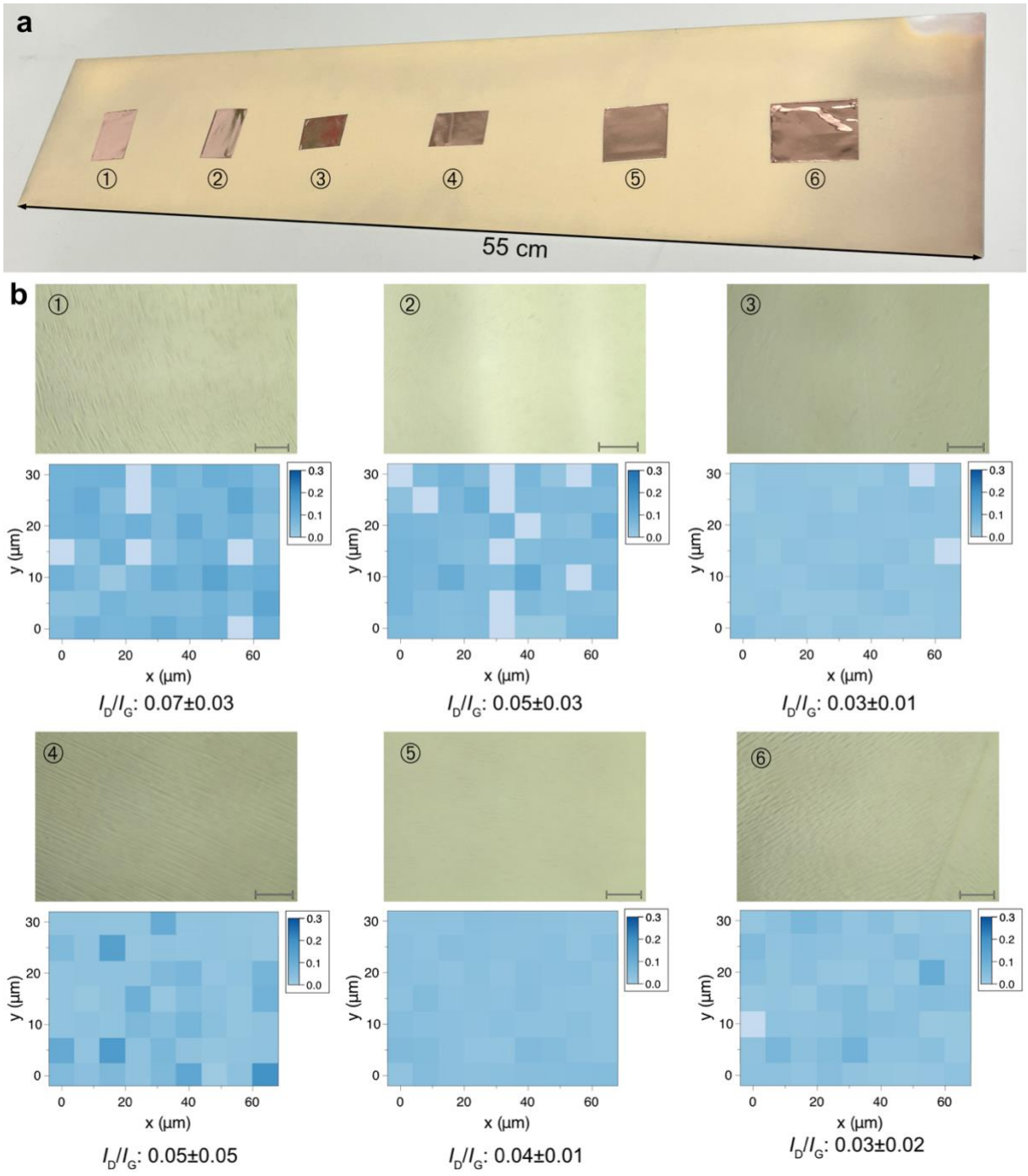

Figure 19. a) Photo of six graphene coupons grown at different positions on the 55 cm long sample plate. b) Optical microscope image (top) and the Raman mapping of D and G peak intensity ratio (bottom) of the graphene sample located at the position of 1, 2, 3, 4, 5, and 6, respectively. The scale bar is 10 μm.

4.4 Uniform oxidation of large-area graphene

From the experimental point of view, in the year 2023, we mainly tried to systematically study pore formation in graphene as we scaled up. Important observations were that the flow uniformity, temperature uniformity, gas velocity, and size of the reaction zone are important parameters in controlling the porosity, and hence the membrane permeance (GPUs), while at the same time, determining as to what size of the sample can be treated by ozone in the reactor. We made several learning by making several reactors (different tube diameters, different heating sources, different temperature uniformity), and based on the results, concluded that the best way to oxidize graphene to form pores in a uniform and scalable way is to use a large diameter furnace where large coupons of graphene (27 cm x 12 cm) can be inserted for uniform oxidation. These activities have improved our success rate in obtaining high-quality membranes (success rate close to 100% for a given process condition). We will continue to optimize the flow of O_3 to obtain maximum reactivity. We will also seek to optimize the reaction at or near room temperature (currently at or near 80 ºC) because we recently learned that oxidation of Cu beneath the graphene film may limit the performance of the membrane (because oxidized Cu is rough and can potentially crack atom-thick graphene film).

Another interesting learning was the management of ozone. At the start of the project, we were storing ozone in a 250 L reservoir tank (Figure 20) to allow injection directly in the CVD reactor after the synthesis of graphene. This allowed the reaction to continue for a certain time with a continuous ozone flow in a large volume of CVD reactor (60 liters), which was otherwise not possible. We have now moved to a smaller reactor volume (thanks to our discovery that a smaller volume with higher ozone velocity is a critical parameter for porosity incorporation), where it is found that a 2 liter/min flow of ozone directly from the ozone generator is enough to induce reaction for porosity incorporation. In this view, we have stopped storing ozone in the tank. This also helps us to manage safety in the lab (in case of a leak of ozone from the tank). We also realized that the concentration of stored ozone in the tank is lower (~4-5%) compared to that generated by the generator (~8%). This could be due to the degradation of ozone in the storage tank. By avoiding storing ozone, we ensured a continuous supply of 8% ozone to the reactor.

Figure 20. Ozone reservoir for a quick injection of ozone into the CVD furnace.

Below is a summary of our optimization.

Optimization in the ⌀5 cm chamber

As shown in Figure 21, we built a 5 cm diameter reaction chamber for ozone optimization to obtain some preliminary data. The sample was first cleaned externally in a tube furnace and then immediately transferred into the reaction chamber. A thermocouple is placed near the sample position to monitor the reaction temperature. Figure 22shows the color change of the sample during the process. After ozone treatment, the oxidation of the substrate is reflected by a darker color change, and it turns back to the original color after reduction. The aspect of color is important and helpful because the oxidized Cu is quite rough. Our attempts to make membranes by skipping the reduction step failed, underlying the importance and need of making the Cu surface smooth by reduction.

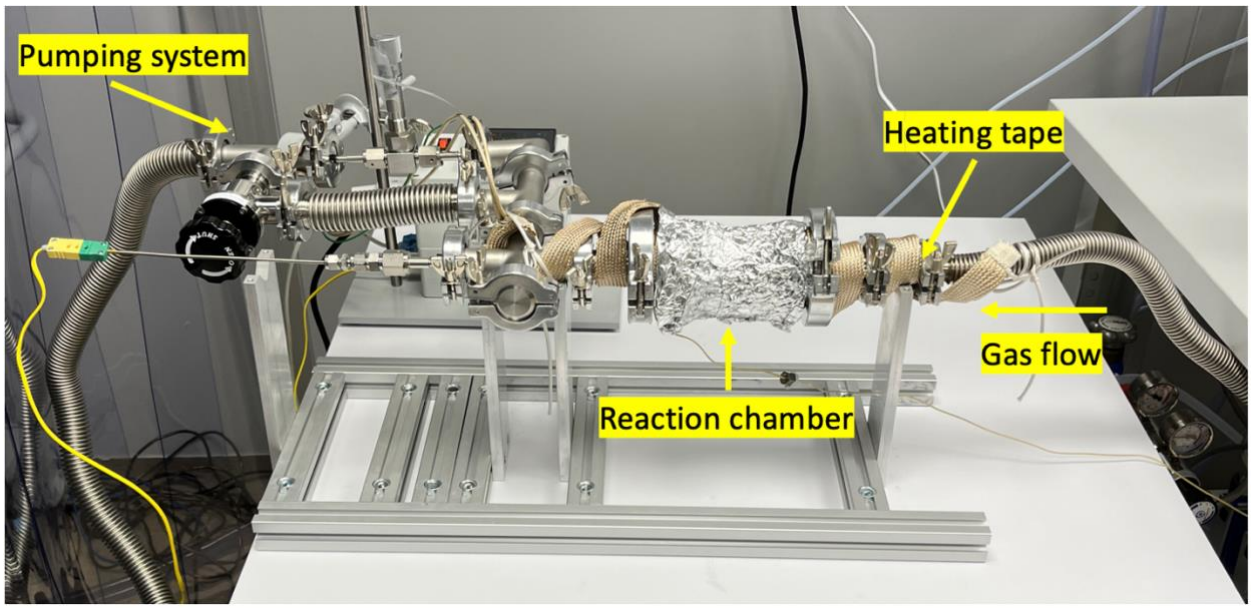

Figure 21. ⌀5 cm chamber for ozone functionalization. The sample is placed inside the reaction chamber.

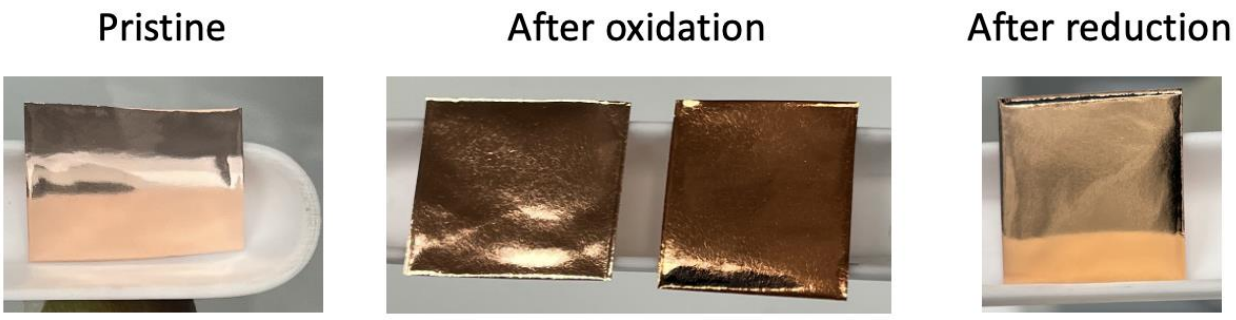

Figure 22. The color change of the sample at different steps of the reaction.

The ozone oxidation was initially conducted at 80 ℃ for 1 h with an ozone flow rate of 500 ml/min. Since the reaction temperature is relatively high, we also applied a stabilization step, which cools the sample with the same ozone flow to room temperature. After oxidation, we transferred and assembled the graphene in our 1-cm membrane module. The extent of ozone oxidation was characterized by the gas permeation study. Figure 23 shows the CO_2 gas permeance and CO_2/N_2 gas pair ideal selectivity of pristine graphene and the graphene oxidized under different conditions. All membranes show a higher

gas selectivity than the supporting layer, reflecting a highly reproducible membrane fabrication strategy we developed in the past years. We observe a noticeable improvement in CO_2 permeance for oxidized graphene, indicating a successful pore formation by ozone reaction. However, the gas selectivity is only marginally improved, and there is a big variation in gas permeance. This shows that the pore etching is not uniform, and the size distribution is broad.

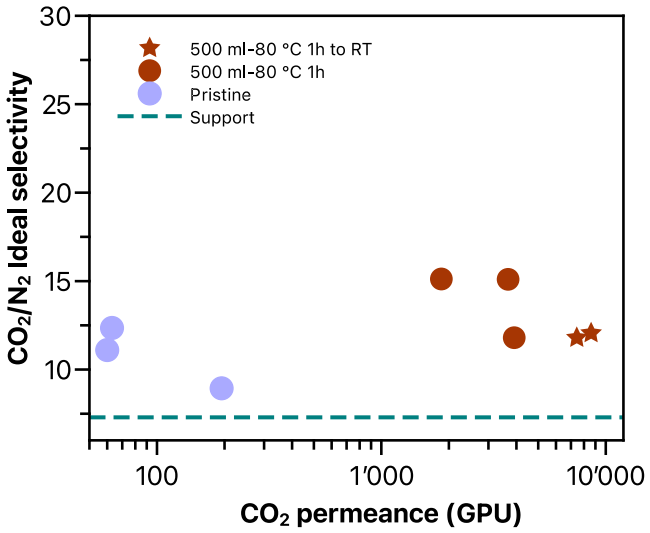

Figure 23. Gas permeation results of the ozone-oxidized graphene from ⌀5 cm chamber.

Optimization in the ⌀16 cm chamber

We upgraded the reaction chamber to a 16 cm-in-diameter tube, aiming to improve uniformity and scalability at the same time (Figure 24), while the experimental procedure stayed the same.

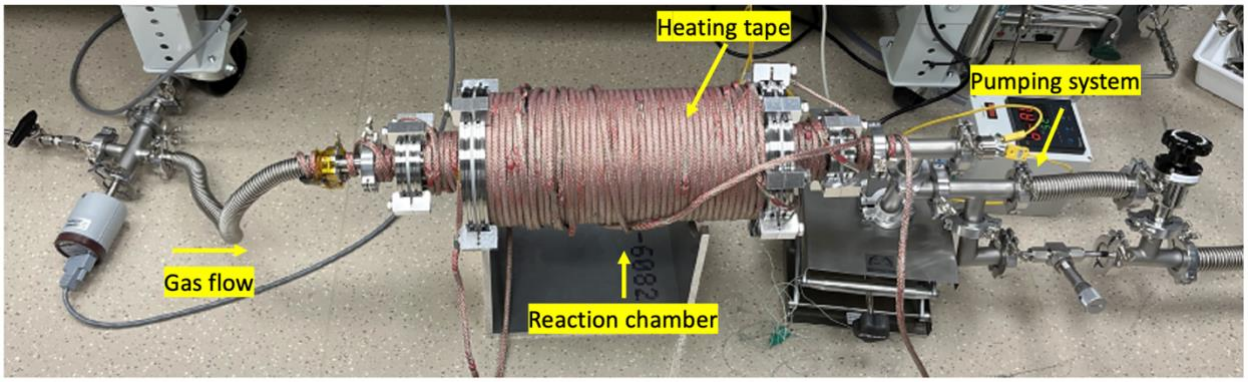

Figure 24. ⌀16 cm chamber for ozone functionalization.

Before optimization, we conducted CFD simulations to understand the gas flow profile inside the reaction chamber. It allowed us to understand the gas flow profile in our specific setup. When we first started to optimize the ozone condition, the reaction chamber was small and we observed that oxidation was not uniform across a large sample. We found from the CFD simulation that it is because of the reaction chamber being too small that we can not have a uniform gas flow profile on top of our sample. Based on the CFD result, we further developed a larger reactor where the gas flow profile is much more uniform.

Figure 25 shows the gas velocity comparison between ⌀5 cm and ⌀16 cm chambers at the same flow rate.

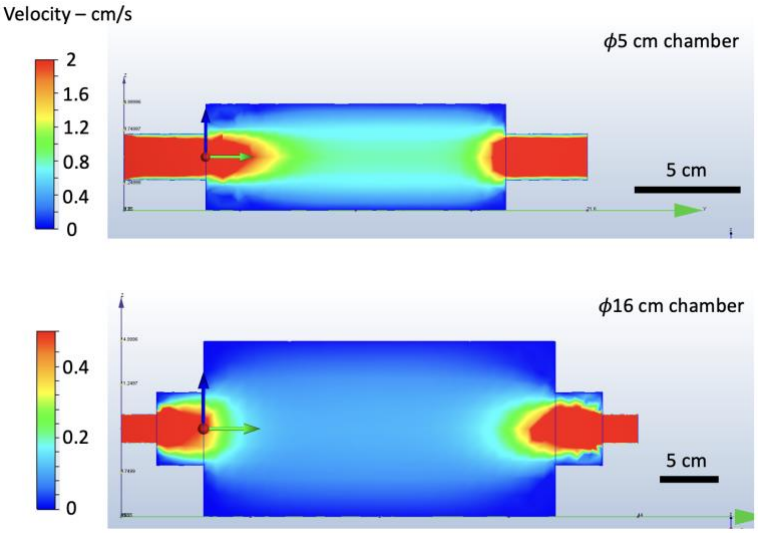

Figure 25. Computational fluid dynamic (CFD) simulation of the gas velocity in different reaction chambers.

It is clear that the gas velocity across the sample is dependent on the geometry of the reaction chamber. Under the same gas inlet flow rate, the ⌀16 cm chamber gives a slow but uniform gas velocity (average gas velocity from the entire reaction chamber: ~0.12 cm/s), while that in the ⌀5 cm chamber is fast but not uniform (average ~1.2 cm/s).

Similar to the ⌀5 cm chamber, we examined the gas permeance of the membrane prepared under the same experiment condition. We observe that the increase in CO_2 permeance becomes less as the reaction chamber diameter increases. Given that the gas velocity in the ⌀16 cm chamber is about 10 times slower than in the ⌀5 cm chamber, the gas velocity could play an important role in increasing the pore density of the oxidized graphene. We further applied a larger gas inlet flow rate for the ozone reaction. The result (Figure 26) shows that the membrane gas permeance varied largely from 5000 GPU to 10000 GPU, close to the permeance of the polymer support (10000 GPU), with a compromise of gas selectivity. The CFD simulation (Figure 27) indicates that as increasing the gas inlet flow rate in the ⌀16 cm chamber, the uniformity of the gas velocity decreases drastically, which makes ozone oxidation difficult to control. We note that the region of interest for the analysis of gas velocity and uniformity is at the center of the reactor which is where the sample is placed.

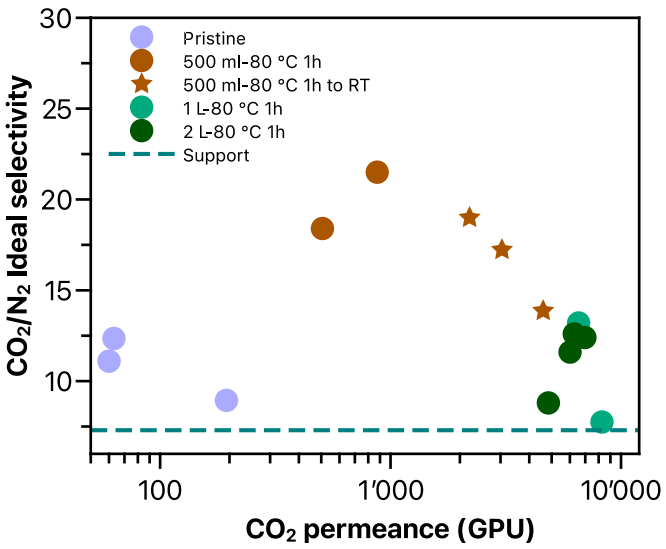

Figure 26. Gas permeation results of the ozone-oxidized graphene from the ⌀16 cm chamber.

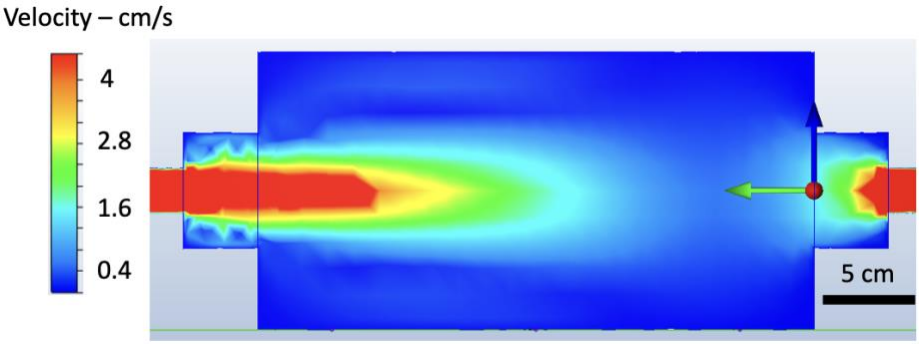

Figure 27. CFD simulation of the gas velocity in the ⌀16 cm chamber with a flow rate of 2 l/min.

Optimization in the ⌀2.5 cm quartz tube furnace

We notice that the uniformity of the gas velocity may depend on the length of the reaction chamber. Figure 28 shows the CFD simulation of the gas velocity in a ⌀2.5 cm quartz tube under 0.5 and 2 l/min. A smaller tube diameter results in a much faster gas velocity. At the same time, the uniformity is also improved, indicated by a thin, slow gas flow near the tube wall and a similar gas velocity in the middle of the tube. The modified setup is shown in Figure 29, and the gas permeance of the membrane oxidized in this setup under the same condition is shown in Figure 30.

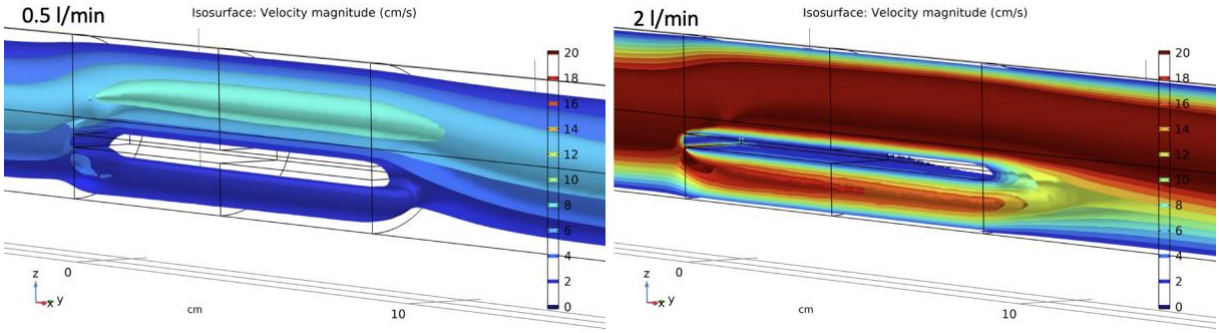

Figure 28. CFD simulation of the gas velocity in the ⌀2.5 cm tube with a flow rate of 500 ml/min and 2 l/min. A sample plate was placed in the reaction chamber.

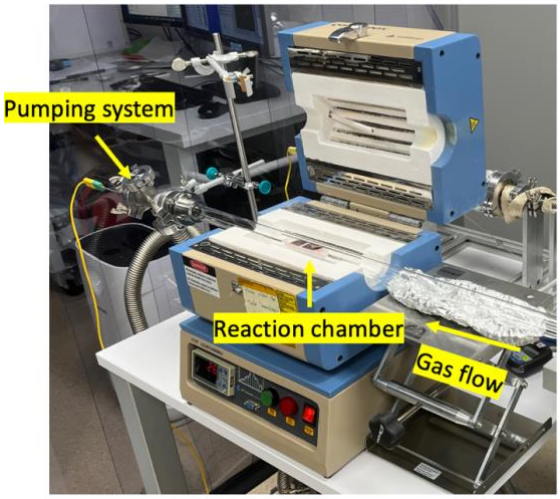

Figure 29. ⌀2.5 cm quartz tube furnace for ozone functionalization.

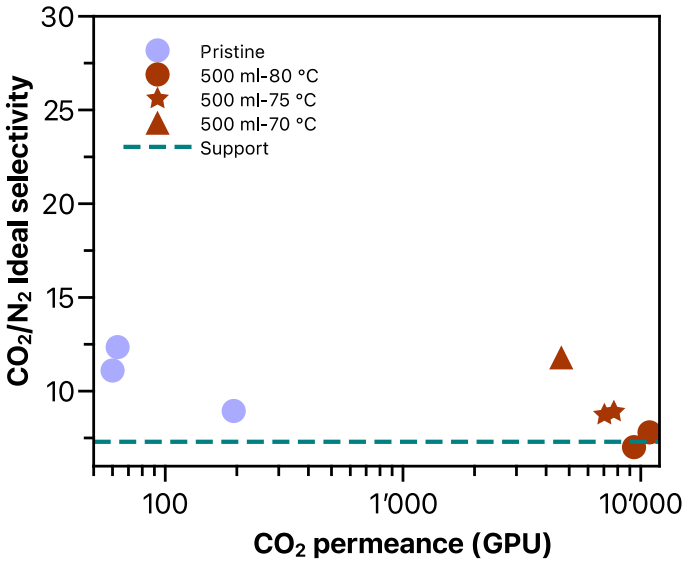

Figure 30. Gas permeation results of the ozone-oxidized graphene from ⌀2.5 cm quartz tube furnace.

The graphene treated under the same condition (flow rate: 500 ml/min, temperature: 80 ℃) shows a defective feature, with both the permeance and the gas selectivity close to the support. The increased oxidation extent on the graphene lattice is attributed to the high gas velocity in the ⌀2.5 cm tube. As we decrease the oxidation temperature, the gas permeance of the membrane goes down, while the selectivity doesn't obviously improve.

Optimization in the ⌀12 cm quartz tube furnace

Considering all the aspects mentioned above, we finally upgraded the oxidation setup in a ⌀12 cm quartz tube furnace. Based on the CFD simulation (Figure 31), we believe the oxidation reaction in this tube furnace is moderate, uniform, and scalable. This is confirmed by the preliminary gas permeation results of the membrane prepared under a flow rate of 2 l/min at 85 ℃. As shown in Figure 32, the CO_2 permeance is averaged around 1000 GPU, and CO_2/N_2 selectivity is about 20.

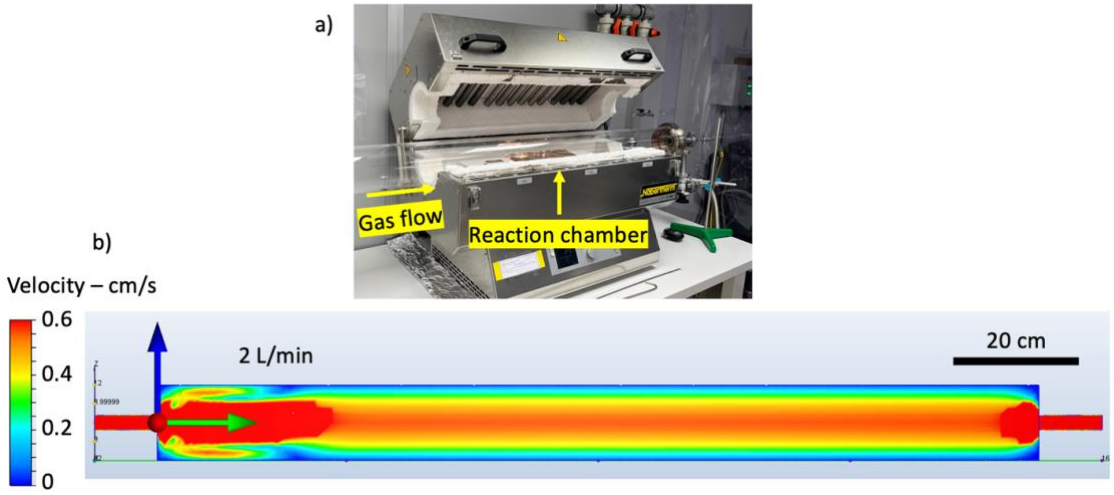

Figure 31. a) Picture of the ⌀12 cm quartz tube furnace for ozone functionalization. b) CFD simulation of the gas velocity in the ⌀12 cm tube with a flow rate of 2 l/min. The gas velocity scale is exaggeratedly zoomed in to show that the gas flow becomes uniform after 30 cm from the inlet.

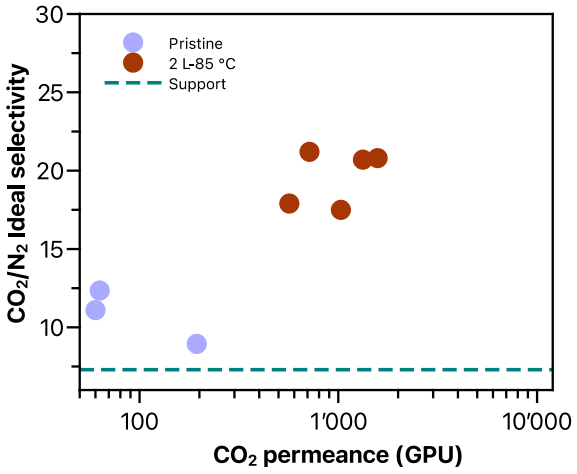

Figure 32. Gas permeation results of the ozone-oxidized graphene from the ⌀12 cm quartz tube furnace.

As we were trying to further improve the membrane performance while preserving the scalability of our reactor, we developed a novel method that alleviated the mass transfer limitation in the O_3-led oxidation reaction. More detailed CFD simulations were performed using COMSOL to understand mass transfer. Figure 33 shows the simulated iso-surface plot of the gas velocity within the above-mentioned reactor (with an inlet flow rate of 2 l/min in the tubular reactor where a substrate holding Cu/graphene was placed).

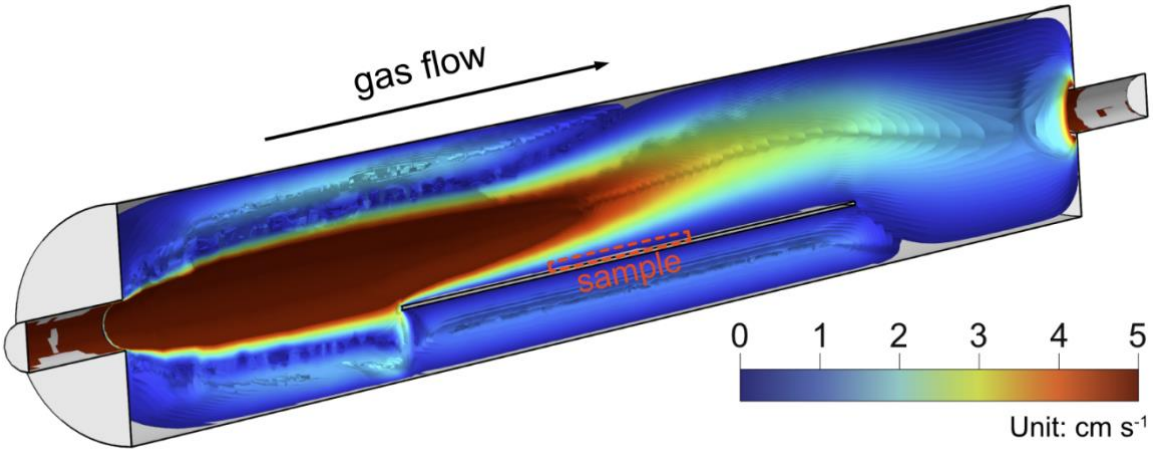

Figure 33. COMSOL simulated gas flow profile: iso-surface plot of gas flow velocity in the reactor with the sample substrate.

The highest velocity was near the center of the reactor. This is because of the small cross-sectional area of the gas delivery system relative to the reactor. The former was essentially a tube with an inner diameter of 2.2 cm. A boundary layer could be observed near the substrate where the gas velocity was significantly reduced. A 2D plot of the gas velocity, 1 mm above the substrate, on a 6 × 16 cm area at the center of the substrate is shown in Figure 34. The influence of the reactor geometry is apparent with varying gas velocity in different parts of the reactor. The gas flow was highest in the center and decreased at the edges of the reactor. The average gas velocity near graphene was 0.06 ± 0.04 cm/s, indicating an uneven flow. A high standard deviation in velocity is not desired for obtaining uniformly porous graphene in scaled-up samples.

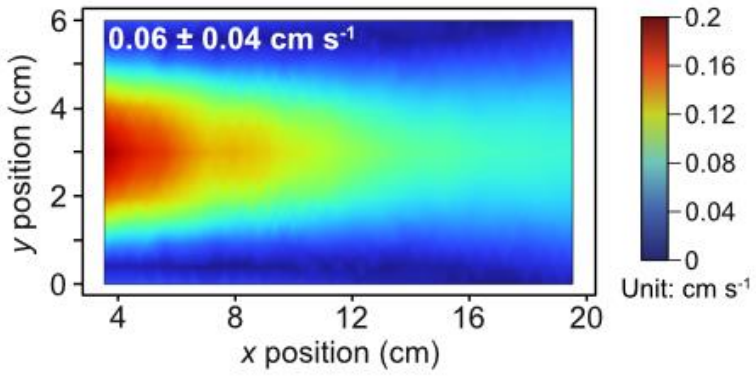

Figure 34. COMSOL CFD simulation results from the unmodified reactor: extracted gas velocity 1 mm above the substrate in the middle of the reactor (see Figure 33) with a sample size of 6 × 16 cm^2.

To address this, a quartz semi-cylindrical block (12 cm in diameter) was placed in the reactor, occupying and blocking the bottom half of the unnecessary space for the ozone reaction. Figure 35 shows the tubular reactor hosting the semi-cylindrical block and a 55 cm-long graphene substrate plate. Attributing to the reduction in the cross-sectional area of the flow by the block, the gas develops a laminar flow at a short distance after the inlet (Figure 36). A 2D plot of the gas velocity near graphene reveals a significantly uniform flow profile (Figure 37). The velocity increased three-fold to 0.17 ± 0.02 cm/s. This led to a significant improvement in the porosity of graphene, reflected by a drastically improved CO_2 permeance. An average CO_2 permeance from the 1-cm-scale membranes of 13105 GPU and CO_2/N_2 selectivity of 15.1 could be achieved. Furthermore, 50-cm^2-sized PG membranes in the 5 × 10 cm^2 cross-flow module yielded attractive separation performance with CO_2 permeance of up to 11799, and CO_2/N_2 selectivity of up to 17.6, respectively (Figure 38, Figure 39). This performance is highly competitive to those from the state-of-the-art and commercial membranes (Figure 40).

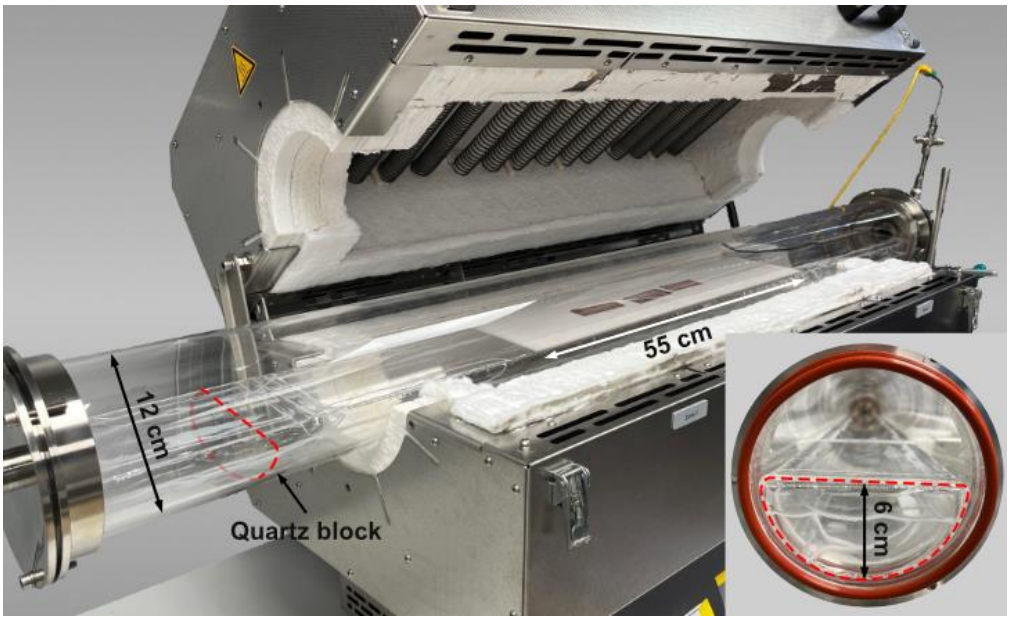

Figure 35. Picture of the modified ozone oxidation reactor hosting a quartz semi-cylindrical block (12 cm in diameter). The inset is the side view of the reactor with the quartz block

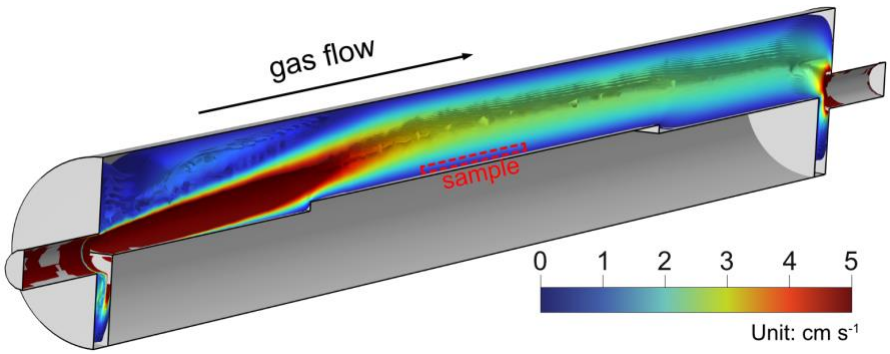

Figure 36. COMSOL simulated gas flow profile: iso-surface plot of gas flow velocity in the reactor with the sample substrate on the quartz block.

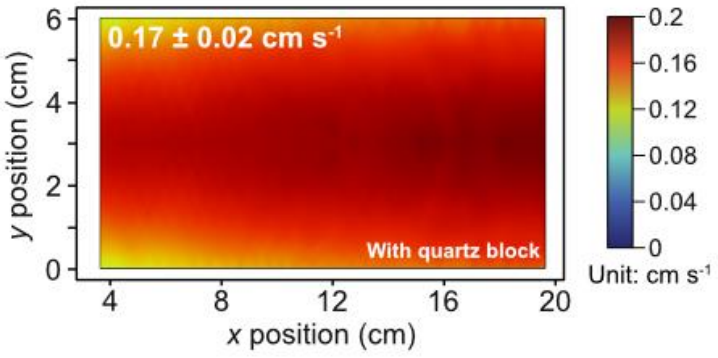

Figure 37. COMSOL CFD simulation results from the modified reactor: extracted gas velocity 1 mm above the substrate in the middle of the reactor (see Figure 36) with a sample size of 6 × 16 cm^2.

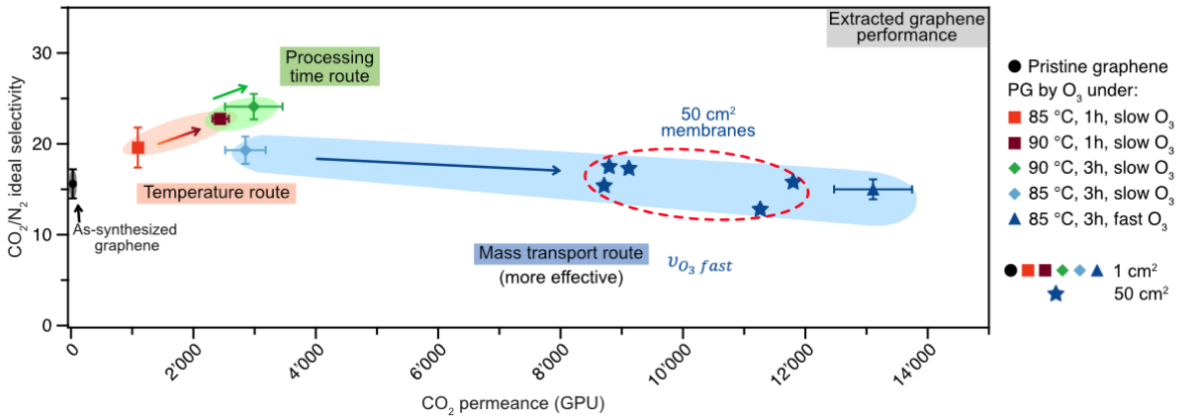

Figure 38. Gas permeation results of as-synthesized graphene (black) and PG (colored) membranes at 1 cm^2 and 50 cm^2-scale. The ozone oxidation was optimized by different reaction routes: temperature, processing time, and mass transport routes. The permeance of PG is extracted from the membrane using the resistance model.

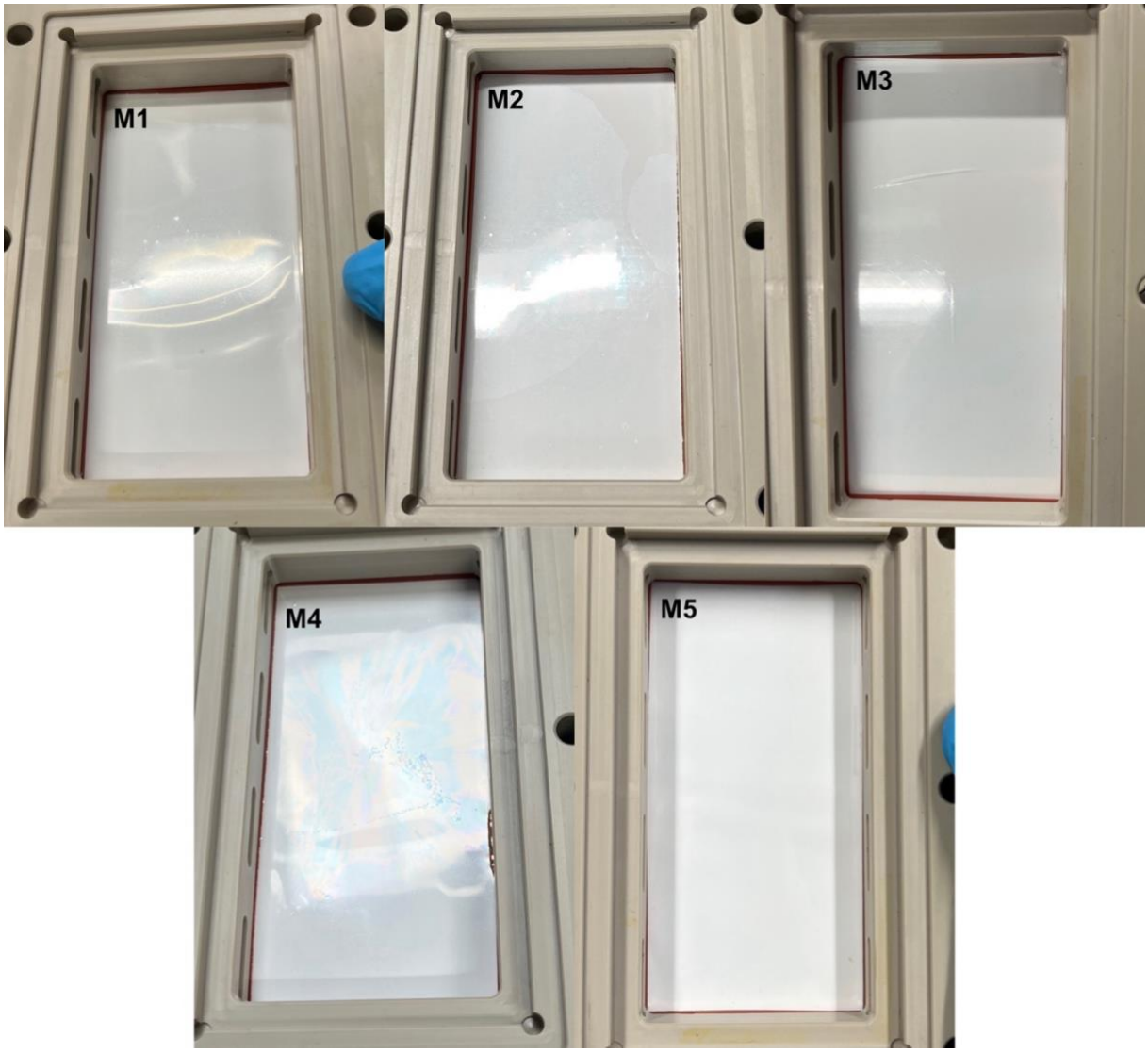

Figure 39. Pictures of five 50 cm^2 porous graphene membranes.

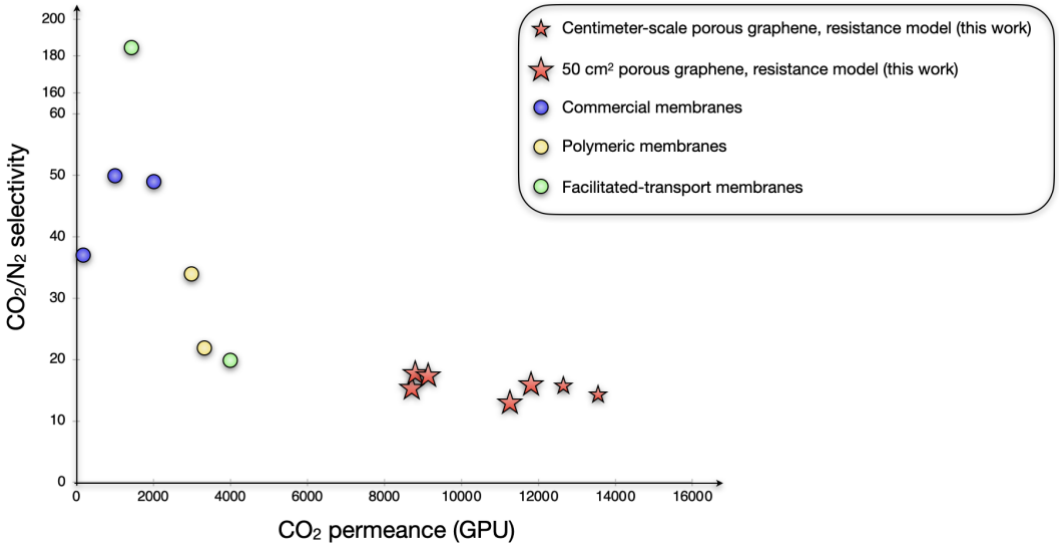

Figure 40. Comparison of carbon capture performance of porous graphene membrane.

AC-HRTEM images of graphene under an oxidation condition using fast and slow ozone gas velocity were collected. Several CO_2-selective pores were observed on porous graphene (Figure 41). Pores formed by missing N carbon atoms are denoted as pore-N, where N is an integer. Pores smaller than pore-10 are considered to be CO_2-impermeable. The density of CO_2-permeable pores under the fast ozone was two times higher than the slow ozone condition (Figure 42). The pore size distribution (Figure 43) shows that the fast ozone velocity is optimal. Above all, a carefully designed scaled-up reactor and transfer strategy allows one to achieve attractive performance from large-area graphene membranes.

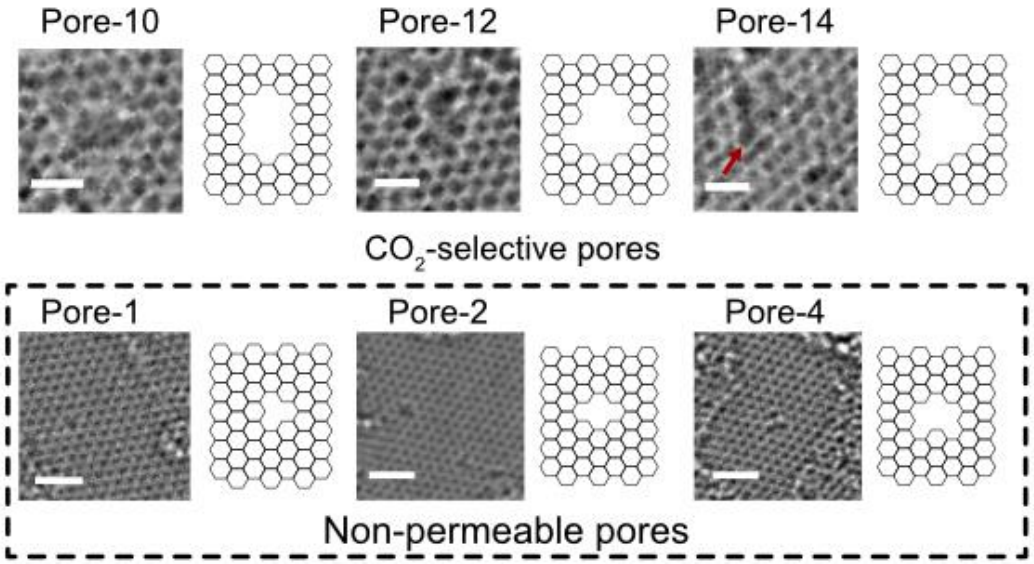

Figure 41. AC-HRTEM images of pores generated under an oxidation condition using fast ozone velocity. Scale bar: 0.5 nm for Pore-10, 12, and 14, 1 nm for Pore-1, 2, and 4.

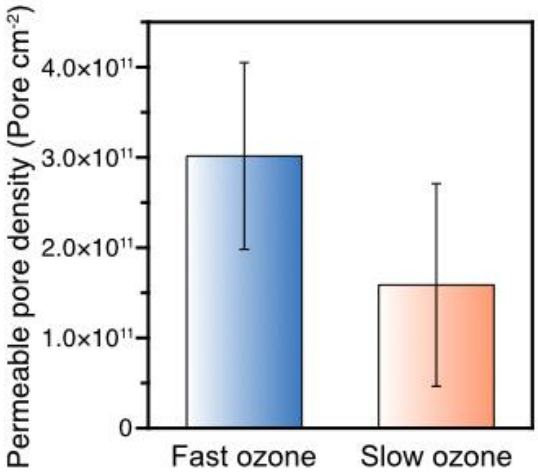

Figure 42. Density of CO_2-permeable pores as a function of the ozone velocity. The error bars represent the standard deviation from 5 AC-HRTEM images.

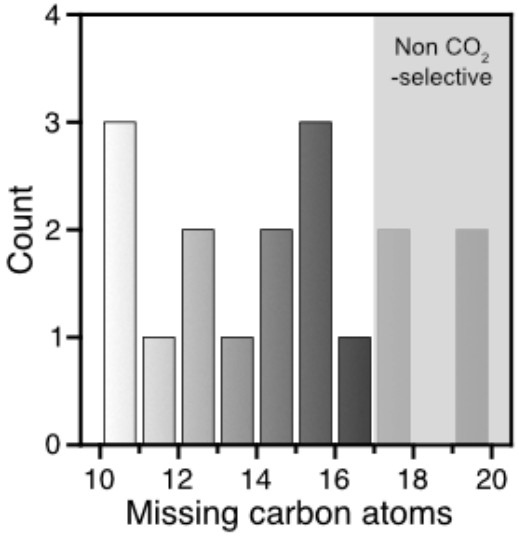

Figure 43. Size distribution of CO_2-permeable pores under fast ozone velocity obtained from the AC-HRTEM images.

4.5 Development of membrane module

Module design – selection of channel thickness to reduce nonideal effects

The practical module would not mimic the design of the centimeter-scale module but rather the plate and frame module shown in Figure 14. It contains two membrane sheets which are separated by a small distance. The selection of the distance between the sheets inside the module is important because this distance corresponds to the thickness of the feed channel, and therefore, it affects the velocity of the stream. The channel thickness is designed in order to reduce two non-ideal effects of the membrane process connected to velocity, i.e., concentration polarization and pressure drops.

With concentration polarization, the concentration of the permeable component at the membrane interface is lower than in the bulk, and this reduces the driving force across the membrane. The

concentration profile along the thickness direction depends on the transport of the component in the channel and on the transport of the component through the membrane. To reduce concentration polarization, we would need a channel as thin as possible since, ideally, the concentration profile in one section should be flat to maximize the driving force. On the other hand, a thinner channel brings higher velocity and higher pressure drops.

When the transport coefficient through the membrane (permeance) is higher, the concentration at the membrane interface is depleted and the concentration polarization is stronger. Therefore, with high permeance, we need to use thinner channels to reduce the concentration polarization, while when the permeance is lower, larger channels can be used.

From a practical point of view, a larger channel thickness is easier to realize and this reduces the pressure drops. Thus, the selected channel thickness is the largest thickness at which the concentration polarization is still limited. We investigated a range of thicknesses between 200 and 1500 µm for a global CO_2 recovery between 50 and 90% (fixed purity of 98%). The process presents two membrane stages, where the second is fed by the permeate produced by the first, and the retentate of the second is recycled and mixed with the feed of the first stage.

We evaluated the impact of channel thickness on the membrane area of the first stage since this typically covers most of the total membrane area (Figure 44). It is evident that the membrane area increases significantly when the channel thickness increases, and this is particularly evident at large recovery values. However, the impact of channel thickness is almost negligible at the lowest investigated recovery (50%).

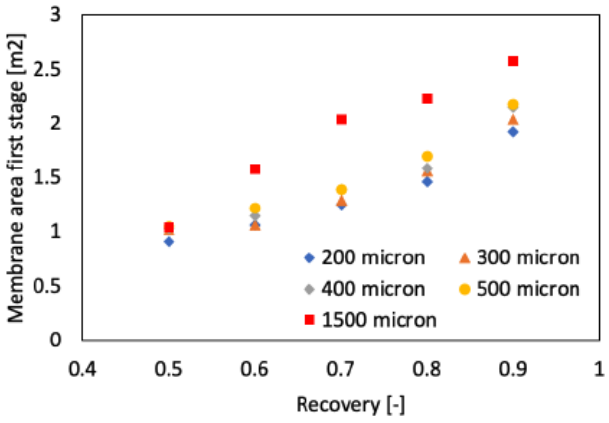

Figure 44. Membrane area in the first stage at variable global recovery and variable channel thickness. Final CO_2 purity target of 98%. Feed pressure in the first stage equal to 3 bar and permeate pressure equal to 0.01 bar. The membranes used for this plot have CO_2 permeance of 1000 GPU and CO_2/N_2 selectivity of 15.

Module design – initial experimental validation with prototype

We applied the same membrane reinforcement strategy and designed a new membrane module to increase the actual membrane area from ~ 1 cm^2 to 10 cm^2, and to 50 cm^2. Figure 45 shows the 3D model of the membrane module, and Figure 46 and Figure 47 show the step-by-step assembly of the 10 cm^2 and 50 cm^2 membranes, respectively.

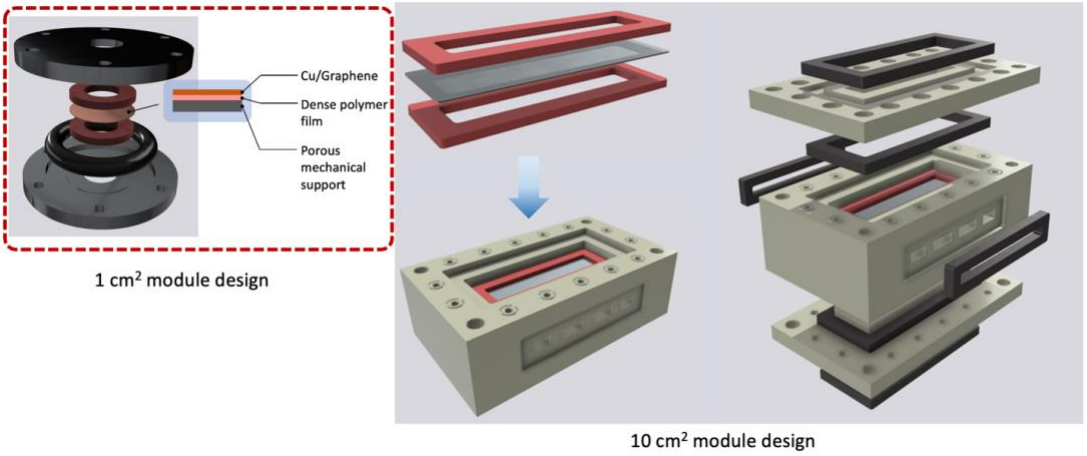

Figure 45. 3D model of the membrane module.

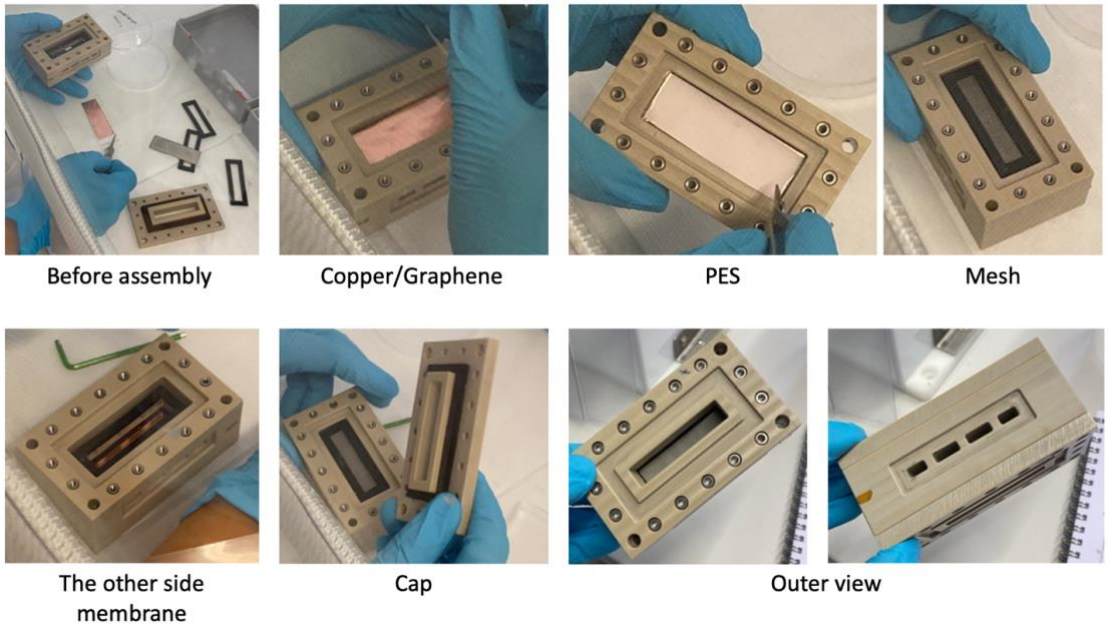

Figure 46. Step-by-step assembly of 10 cm^2 membrane module.

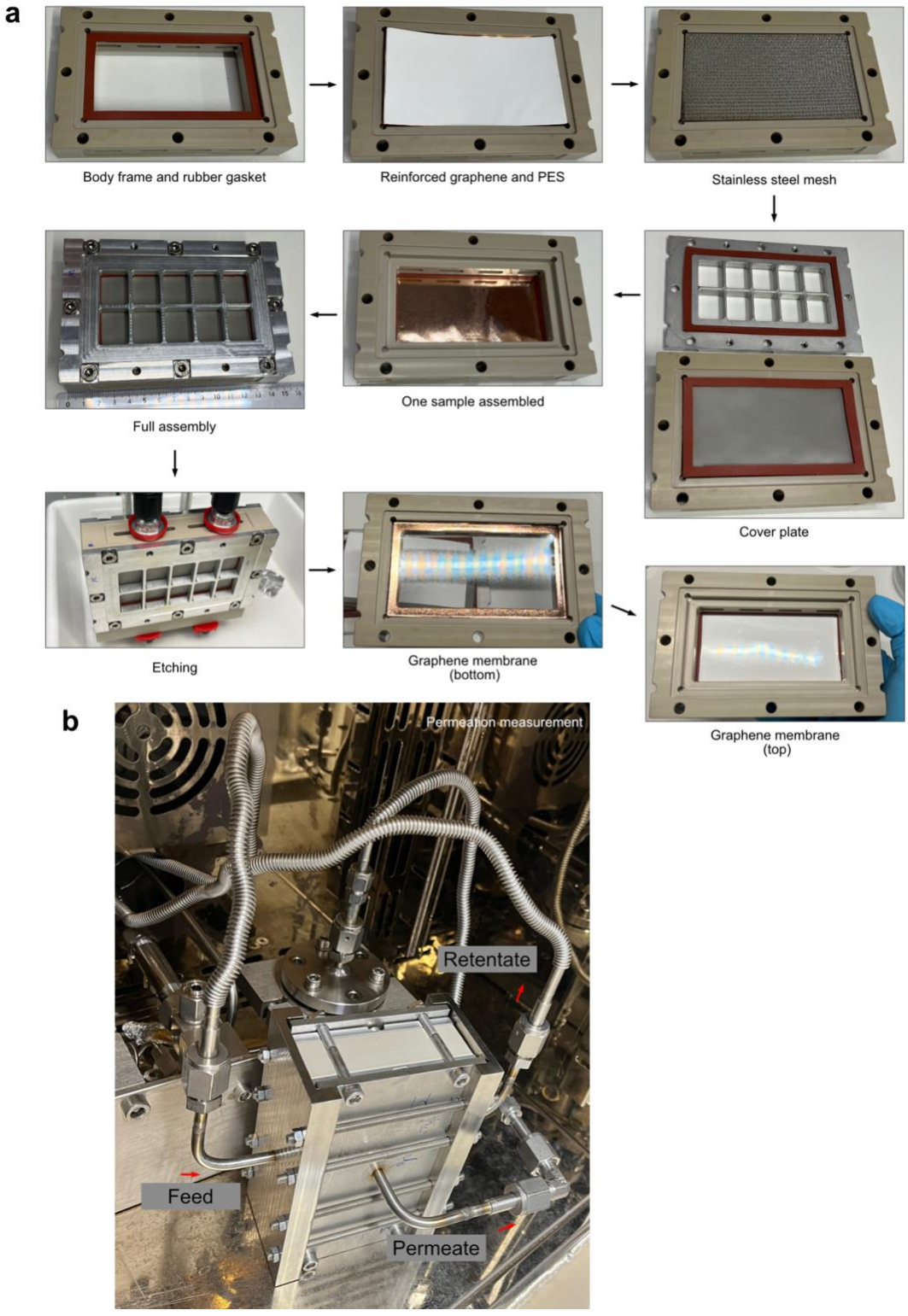

Figure 47. a) A step-by-step fabrication of 5 × 10 cm^2 graphene membrane using the modified membrane module, and b) pictures of the module for gas permeation measurement.

In our first prototype (Figure 45), there is a large (~9.6 mm) gap between the two membrane elements assembled in the module on the feed side of the membrane. As expected from the modeling section, this led to an issue with concentration polarization when the feed gas is a mixture of CO_2 and N_2 at a CO_2 permeance of 1000 GPU. To solve this, we reduced the gap in the feed channel gap to 1.6 mm by placing a rectangular block inside the membrane module (Figure 48). Figure 49 shows the resulting normalized CO_2 permeance as a function of CO_2 feed concentration from a commercial polydimethylsiloxane (PDMS) membrane with different feed channel thicknesses. It is clear that the concentration polarization effect is reduced when the sample gap becomes thinner. In the next step, we will design a membrane module with an even thinner gap (e.g., 0.3 mm) to avoid concentration polarization.

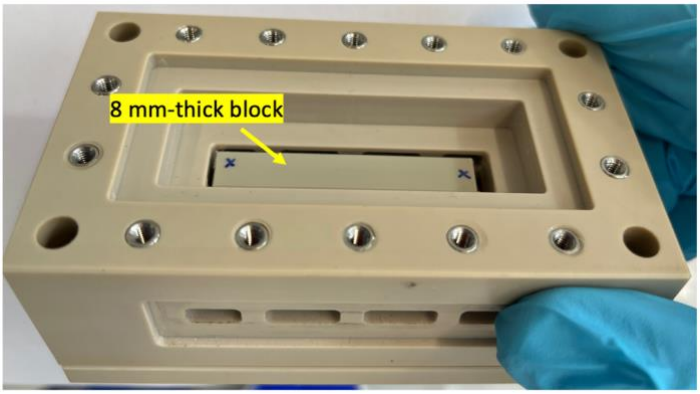

Figure 48. The block stuck in the membrane module to reduce the concentration polarization effect.

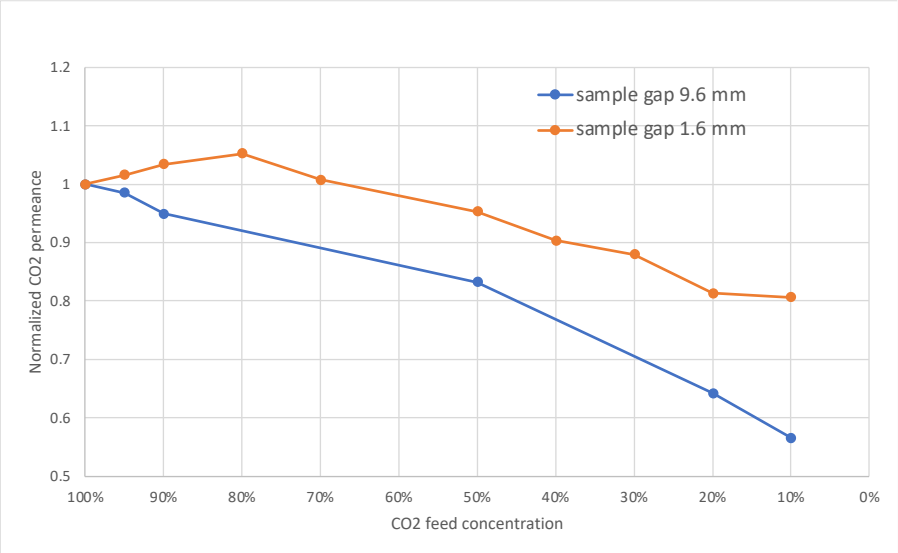

Figure 49. Normalized CO_2 permeance as a function of CO_2 feed concentration obtained from the same membrane with different feed channel thicknesses

4.6 Process design for pilot plant

We performed a techno-economic analysis of double-stage membrane processes for carbon capture from flue gas and from biogas. The technical model designs the process, i.e., estimates the membrane

areas in each stage and the energy consumption of the vacuum pumps and the compressors for a given target of recovery and purity. The model requires a number of inputs and parameters, such as the composition and flow rate of the inlet feed stream, the efficiency of pressure equipment, and the membrane performance parameters. Then, the economic model calculates the capital and operating expenses, where the capital expenses are given by equipment costs, indirect costs, and contingency and fee costs, whereas the operating expenses are given by energy costs, fixed operating costs, and membrane replacement costs. The sum of the capital and operating expenses per year divided by the amount of CO_2 produced per year returns the capture penalty.

The techno-economic model can also identify the set of operating conditions (in particular, the pressures in the feed and permeate channels) that minimize the capture penalty.

Capture from flue gas

We considered various scenarios to include the variation of (i) membrane CO_2 permeance and CO_2/N_2 selectivity; (ii) membrane cost; and (iii) target of CO_2 purity. In particular, we used:

(i) Current membrane permeance and selectivity of 1000 GPU and 15, and future membrane permeance and selectivity of 10000 GPU and 30;

(ii) Conservative cost estimation of 500 $/m^2 and updated cost estimation based on lower-cost copper foil and mesh for support of 100 $/m^2;

(iii) Target purity of 90% and 98%, depending on the downstream process (either storage or utilization).

The simulations take into account a wet feed stream, saturated with water vapor at 50 °C and with an inlet CO_2 concentration of 11.8%. The simulations refer to a large-scale system with a capture rate of around 0.5 million tons per year and a target recovery of 90%.

With CO_2 permeance of 1000 GPU and CO_2/N_2 selectivity of 15, we found that a double-stage membrane process with the combination of feed compression and permeate under vacuum in the first stage is preferable to a process where the driving force relies only on vacuum in the permeate channel. This is because the permeance is relatively low, and when feed is compressed, the membrane area is always reduced. In particular, the optimal configuration presents feed and permeate pressures in the first stage of 5 and 0.08 bar and in the second stage of 1 and 0.1 bar.

The specific energy consumption is equal to 2.52 MJ/kgCO_2 for a purity of 90% and 4.98 MJ/kgCO_2 for a purity of 98%. The energy consumption increases with purity because higher recycle rates of the second retentate are needed. Mostly driven by the increase in energy consumption (Figure 50), the capture penalty increases from 87.2 to 153.4 $/ton, when purity increases from 90% to 98%.

When membrane cost reduces from 500 to 100 $/m^2, capture penalty is equal to 69.5 and 129.5 $/ton, for purity of 90 and 98%, respectively.

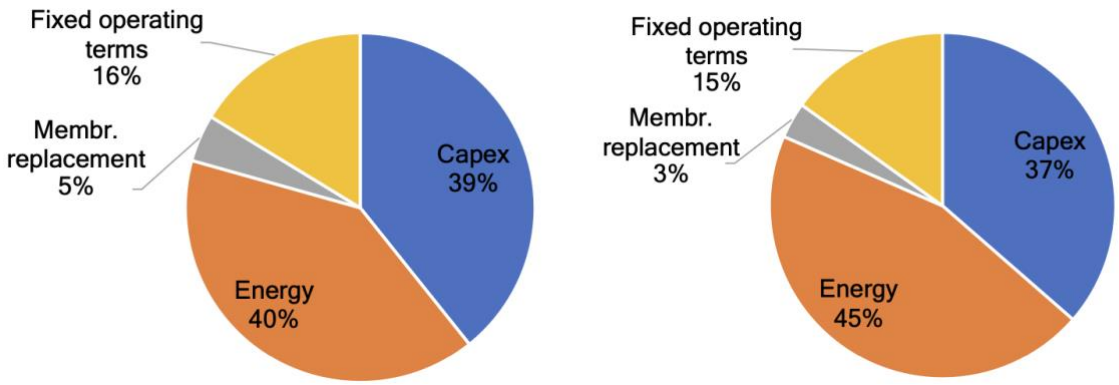

Figure 50. Break-down of capture cost with purity target of 90% (left) and 98% (right), with CO2 permeance of 1000 GPU and CO_2/N_2 selectivity of 15 and with membrane cost of 500 $/m^2.

The capture penalties significantly reduce with the target performance; with CO_2 permeance of 10000 GPU and CO_2/N_2 selectivity of 30 (performances already achieved in our lab at the centimeter scale), a double-stage membrane process with vacuum in the permeate of both stages and ambient pressure in the feed channel is more economically competitive. The selected configuration presents permeate pressures of 0.05 bar in the first stage and 0.1 bar in the second stage. The energy consumption is 1.03 MJ/kgCO_2 and 1.64 MJ/kgCO_2 with purity of 90 and 98%, respectively. As in the previous case, capital costs and energy costs cover almost the same share of the total cost (~ 40%, see Figure 51). The total capture penalty in this case is very attractive and equal to 35.6 $/ton for 90% purity and 52.8 $/ton for 98% purity.

Membrane cost covers between 34 and 37% of the capital costs and the reduction of the specific membrane cost from 500 to 100 $/m^2 leads to a reduced capture penalty of 25.4 $/ton (90% purity) and 39.6 $/ton (98% purity).

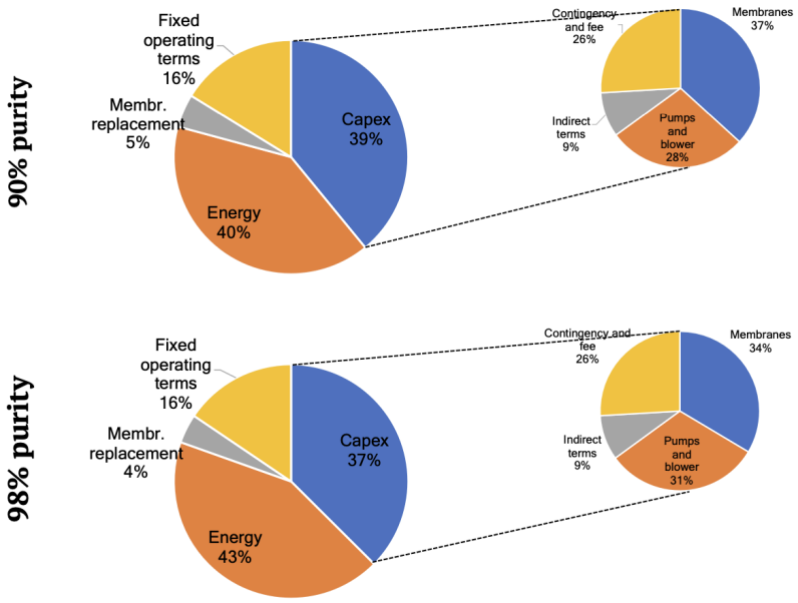

Figure 51. Break-down of total cost and capital cost for capture from flue gas with purity target of 90% (up) and 98% (down), with CO2 permeance of 10000 GPU and CO_2/N_2 selectivity of 30 and with membrane cost of 500 $/m^2.

Capture from biogas

For the simulations of the capture process from biogas, we considered the variation of membrane cost (100 and 500 $/m^2) and of CO_2 permeance (1000 and 10000 GPU), while the CO_2/CH_4 selectivity is fixed at 20 and the purity targets are 90% for CO_2 in the permeate from the second stage and 96% for CH_4 in the retentate from the first stage.

The simulations take into account a bicomponent feed stream (CO_2/CH_4), with an inlet CO_2 concentration of 45%. The simulations refer to a large-scale system with a capture rate of around 0.5 million tons per year.

The selected configuration consists of a double-stage membrane process with a permeate channel under vacuum in both stages (0.05 bar in the first and 0.2 bar in the second) and ambient pressure in the feed channel.

In the case of lower permeance (1000 GPU), the capital cost and the energy cost cover a similar share of the total, even if the specific energy cost is high (0.17 $/kWh compared to 0.05 $/kWh used for capture process from power plant flue gas). It is also worth noting that membrane cost covers more than half of the total capital cost, because of the larger membrane area required at lower permeance (Figure 52).

In this case, the capture penalty is equal to 78.2 $/ton with a specific membrane cost of 500 $/m^2 and it reduces to 45.7 $/ton with a specific membrane cost of 100 $/ton. Conversely, in the case of higher permeance (10000 GPU), energy cost is much higher than any other term (share ~ 77%, see Figure 52 down), and within the capital costs membrane cost covers only 25% of the total.

It is worth noting that the specific energy consumption is the same for the two membranes because selectivity is fixed, and this is equal to 0.68 MJ/kgCO_2. Highly attractive capture penalties of 41.6 and 38.3 $/ton are calculated with a permeance of 10000 GPU and specific membrane cost of 500 and 100 $/m^2, respectively.

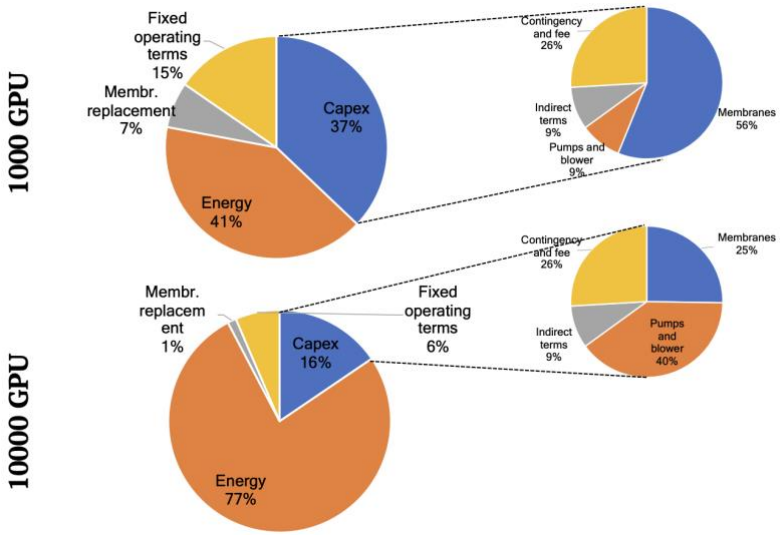

Figure 52. Break-down of total cost and capital cost for capture from biogas with CO_2 permeance of 1000 GPU (up) and 10000 GPU (down), with CO_2/CH_4 selectivity of 20 and with membrane cost of 500 \$/m^2.

Module design – impact of channel thickness

An important aspect to consider especially with highly permeable membranes is the impact of non-ideal phenomena, i.e., pressure drops and concentration polarization. These can be limited by a proper design of the module and in particular by selecting properly the thickness of the feed channel. Generally speaking, the thinner the channel, the smaller the concentration polarization, but also the larger the pressure drops. Therefore, we usually select the smallest channel thickness which allows us to keep the pressure drops below the threshold of 0.1 bar/m.

The selection of the thickness depends on the membrane parameters, especially on permeance, because higher permeance corresponds to larger fluxes through the membrane that causes stronger CO_2 depletion at the feed-membrane interface, i.e., stronger concentration polarization. With this regard, in Figure 53, we show how the required membrane area and the concentration polarization index vary with the channel thickness for the two generations of membranes presented above. In all cases, the pressure drops are below 0.1 bar/m.

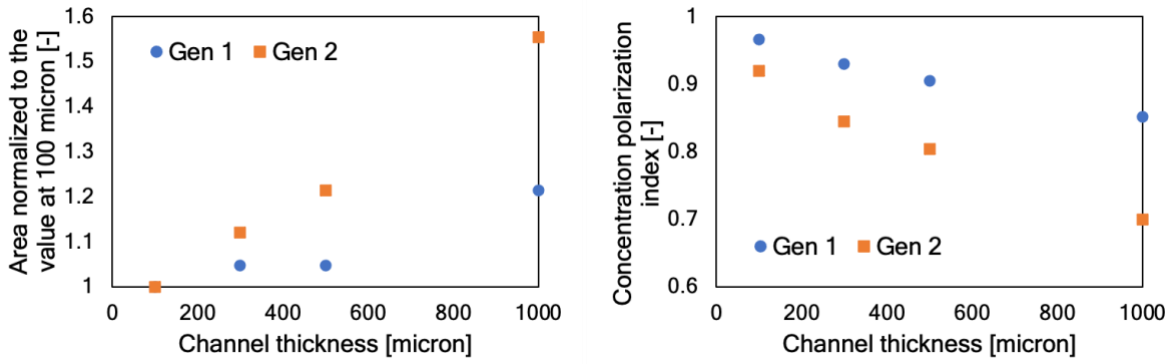

Figure 53. Impact of channel thickness on the membrane area (expressed as normalized area to the value found with channel thickness of 100 μm) and on the concentration polarization index (defined as the ratio between the concentration of CO_2 at the feed-membrane interface and the concentration in the feed bulk).

First, the membrane area required for the same targets of recovery and purity increases when channel thickness increases, because the effect of concentration polarization is stronger. This causes a decrease in the partial pressure driving force; thus, a larger membrane area is required for the same separation. The membrane area increases by around 20% and 60% when the channel thickness increases from 100 to 1000 μm with Generation 1 and 2 membranes, respectively. Generation 2 membranes are more impacted by the variation of channel thickness because of the higher permeance.

This is also evident from the chart reporting the concentration polarization index as a function of the channel thickness. The concentration polarization index is defined as the ratio between the concentration of CO_2 at the feed-membrane interface and the concentration in the bulk of the feed channel. The lower the index, the stronger the concentration polarization.

In line with what is already said for the variation of membrane area, the index decreases when the channel thickness increases and it goes down to 0.85 and 0.7 with Generation 1 and 2 membranes, respectively.

Overall, in order to reduce the loss of driving force due to concentration polarization, we should keep the channel thickness as low as possible while fulfilling the requirement for maximum pressure drops.

Process design and techno-economic analysis

We carried out the optimization of membrane processes for carbon capture by taking into account variable membrane performances (permeance and selectivity) in line with those found in the lab.

All simulations target 90% CO2 recovery and 95% CO_2 purity in the permeate stream, starting from a wet flue gas saturated with water vapor at 50 ºC and with a CO_2 concentration of 11.8%. The cost analyses refer to large-scale processes aiming at producing around 0.5 million tons of CO_2 per year. The main cost assumptions used for the simulations are reported in Table 3.[4]

Table 3. Main economic variables.

Cost variable	Value
Membrane cost [$/m^2]	100
Electricity cost [$/kWh]	0.05
Membrane replacement rate [y]	5
Contingency factor [-]	0.15 (project) + 0.2 (process)
Capital charge factor [-]	0.125
Vacuum pump efficiency [-]	0.7
Compressor efficiency [-]	0.85

All simulations refer to a double-stage process, where the partial pressure driving force is generated by the combination of feed compression and permeate under vacuum in the first stage, whereas in the second stage, the feed channel is at ambient pressure and the permeate channel is under vacuum (see Figure 54). The optimization variables are the pressures in the feed and permeate channels of the first stage and the permeate pressure in the second stage.

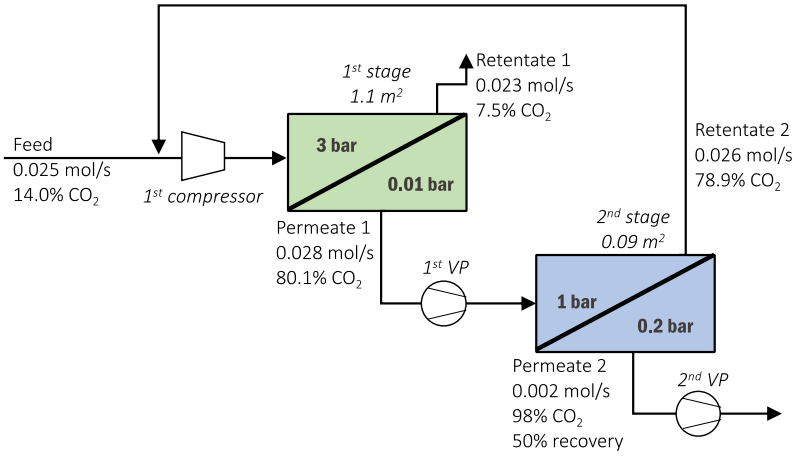

Figure 54. Scheme of the double-stage membrane process for 50% CO_2 recovery from dry feed with CO_2 purity of 98%.

The feed pressure generated in the compressor can range from 1 to 6 bar, whereas the permeate pressures are free to vary between 0.1 and 0.3 bar. In these analyses, we did not consider vacuum pressures below 0.1 bar as a higher vacuum is generally considered more difficult and expensive to realize at a large scale.

The variation of membrane performance parameters corresponds to important variations in overall cost, membrane area, and energy consumption.

We consider two membranes: (i) generation 1 with a CO_2 permeance of 1000 GPU and CO_2/N_2 selectivity of 20, and (ii) generation 2 with a CO_2 permeance of 10000 GPU and CO_2/N_2 selectivity of 50. In both cases, the CO_2/O_2 and the CO_2/H_2O selectivity are taken equal to 12.6 and 1, respectively. The optimal pressure configurations are presented in Table 4. Sets of pressure that minimize capture cost with the two generations of membranes. and the relevant results of the economic analysis are reported in Figure 55.

Table 4. Sets of pressure that minimize capture cost with the two generations of membranes.

	Membrane generation 1	**Membrane generation 2**
Feed channel 1	2.5	1.5
Permeate channel 1	0.1	0.1
Permeate channel 2	0.1	0.2

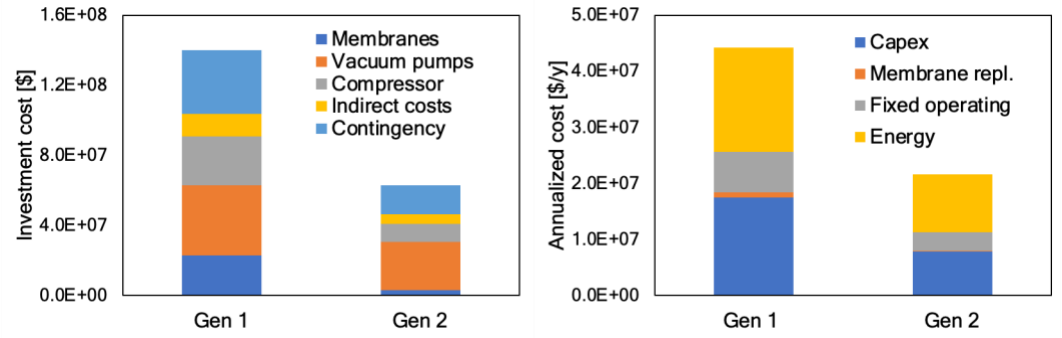

Figure 55. Results of the cost optimization with the two generations of membranes.

Generally speaking, the costs are much higher with Gen 1. In the investment costs, the difference is mostly driven by the membrane cost due to the different values of CO_2 permeance. Conversely, the lower selectivity of Gen 1 membranes causes an increase in energy consumption, because larger recycle rates are needed to achieve the same targets.

The total minimized capture penalty varies from 65.5 $/ton with Gen 1 membranes to 31.0 $/ton with Gen 2, and the specific energy from 2.0 to 1.1 MJ/kg. The capture penalty and the energy consumption with Gen 2 membranes are highly competitive with state-of-the-art polymeric membrane-based processes.

5 Evaluation of results to date

Overall, there has been significant progress since the start of the project, reflected by the successful design, commissioning, and validation of (i) a large-scale CVD reactor to produce graphene, (ii) an oxidation reactor to generate controlled porosity in large-area graphene, and (iii) testing and validation of large-area membranes for CO_2/N_2 separation. Our success rate in producing porous graphene and porous graphene membranes is now near 100%, thanks to the novel transfer-free membrane preparation step developed for larger area modules. We show that porosity in graphene is incorporated by ozone treatment successfully inside the reactor, making it convenient to prepare large-scale (27 cm x 12 cm) porous graphene films on a routine basis. We have validated cross-flow modules with an area of 10 cm^2 followed by an area of 50 cm^2. The process for separation has been optimized inside the scale-up reactor, learning from the conditions for small-scale membranes. The membranes produced by the large-scale reactor shows promising performance with permeance from 50 cm^2 graphene membrane reaching close to 10000 GPU based on the resistance model. We have now also carried out month-long stability testing of a 50 cm^2-sized coupon under laboratory gas flow, which shows stable performance (Figure 56). A slight decrease in permeance over time was observed, which can be attributed to the clogging of graphene pores by contaminants. Based on study over three-month long test in the laboratory, we have shown that this clogging is reversible. Indeed, heating the membrane to 130 ºC for 1 h recovers the permeance of the membrane (see regeneration in Figure 56).

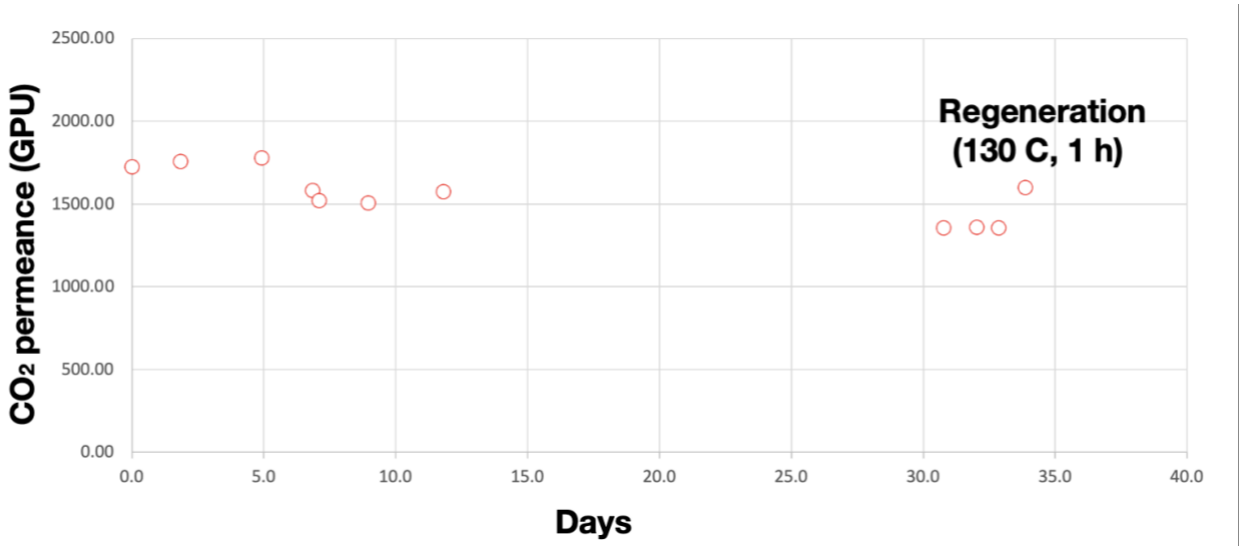

Figure 56. Month-long permeation testing of 50 cm^2 sized graphene membrane showing stable performance.

Key insights, challenges, and measures

One of the key advances in this project is that our success rate in producing graphene membranes is now close to 100%. We have achieved this owing to several factors. These include consistent quality of graphene produced by CVD, and extremely uniform oxidation of graphene in the scaled-up reactor setup thanks to improved mass transfer and uniform velocity, and finally, a novel membrane transfer process which allows crack-free transfer of large-area membranes.

We have taken a decision to carry out oxidation at low (or even room temperature) to improve the scalability and uniformity of the method. This is one of the reasons for achieving a nearly 100% success rate in membrane production, as mentioned above. However, at low temperatures, oxidation kinetics is sluggish compared to high-temperature oxidation. We have explored improving the mass transfer of ozone by improving the velocity of ozone, as indicated by the extensive data on velocity generated in this project. The results are highly encouraging, with extremely promising results at room temperature oxidation by simply increasing ozone velocity (Figure 57 and Figure 58). We have now adapted this results for our project on roll-to-roll fabrication of graphene membranes where oxidation is designed at room temperature, reducing the process complexity.

We are also making progress in industrial testing of the membrane. The deployment of a pilot plant at the Agile site of GAZNAT (See section 7 for more details) has provided valuable operational feedback on the current skid design. Notably, the modularity has proven effective for rapid installation and troubleshooting. Mechanical integration was smoother than anticipated, though thermal insulation around certain fittings needs redesign to reduce water condensation during colder months. Lessons from onsite handling have led to considerations for more compact and transportable configurations leading to an improved skid as shown in Figure 10

A spinoff on graphene membrane (Divea) has been created which is testing membrane stability and performance under various conditions. They have shown stability of membranes in 50 ppm SOx (data not shown).

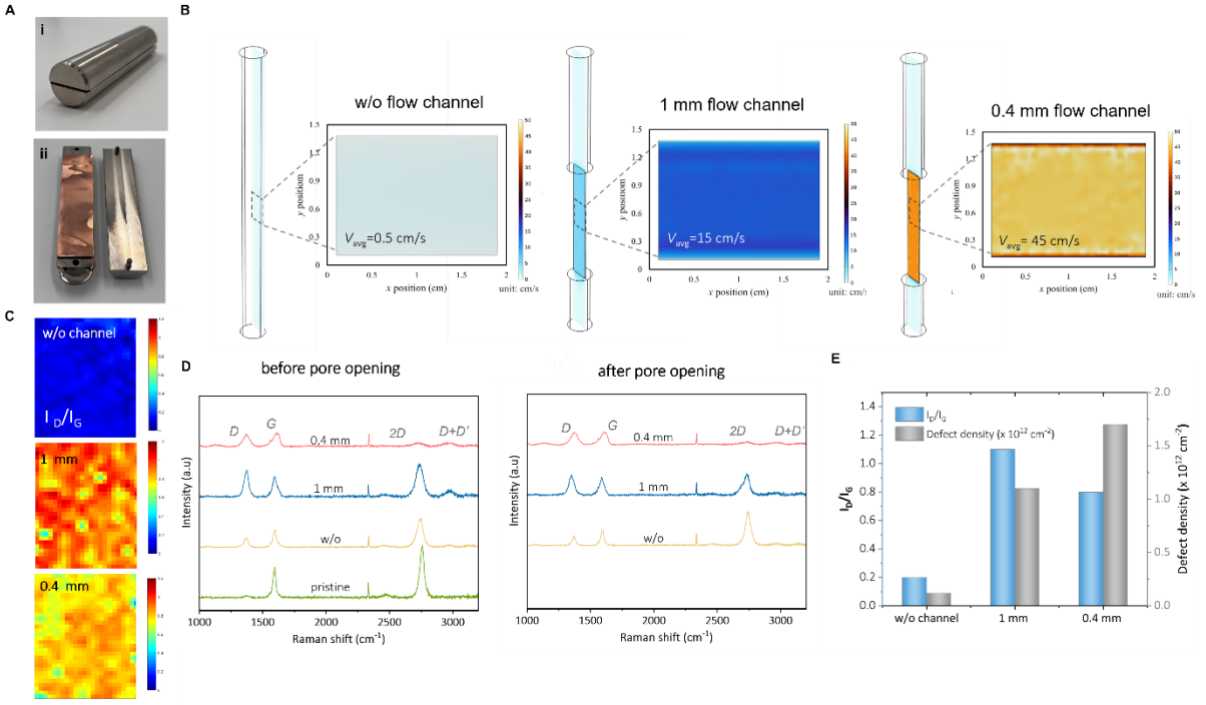

Figure 57. (A) Custom-made flow channel with 1 mm flow gap (i) assembled (ii) before sandwiching the graphene sample. (B) 3D models and 2D velocity profiles of O_3/O_2 flow on 1 mm above the graphene obtained with COMSOL for three conditions: without a flow channel, with a 1-mm flow channel, and with a 0.4-mm flow channel (C) Raman spectroscopy mapping of I_D/I_G for samples exposed to ozone flow under different conditions: without a flow channel, with a 1-mm flow channel, and with a 0.4-mm flow channel (D) Raman spectra of pristine graphene and ozone-treated samples at room temperature, comparing conditions without a flow channel and with 1-mm and 0.4-mm flow channels, both before and after pore opening (E) The change in the I_D/I_G ratio and defect density, analyzed based on the carbon amorphization trajectory, for samples exposed to ozone and light under different oxidation conditions.

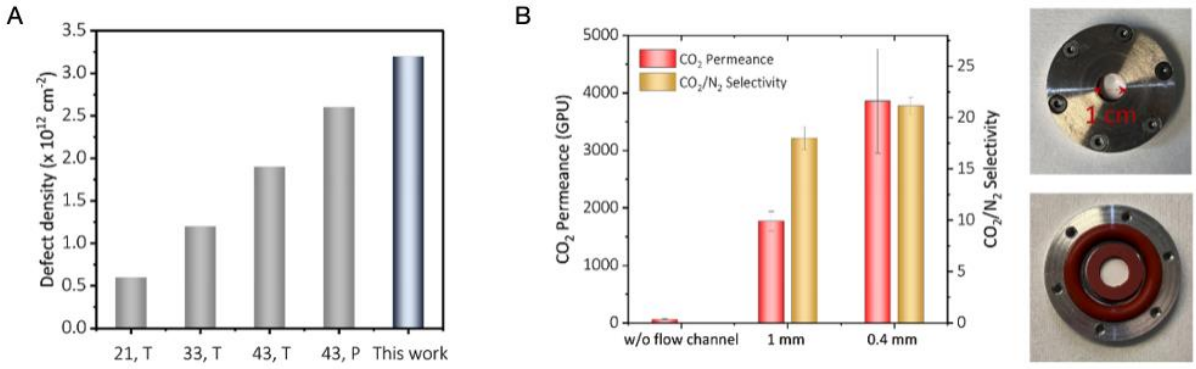

Figure 58. (A) Comparison of oxidative etching using high-temperature and room temperature protocols. Membranes are labeled based on oxidation temperature (°C) and pore incorporation technique, where T represents thermal gasification (heating the samples) and P represents photonic gasification (light exposure). (B) Membrane separation performance of cm-scale membranes, prepared from oxidized graphene samples under different flow conditions: without a flow channel, with a 1-mm flow channel, and with a 0.4-mm flow channel. The right panel shows the pictures of membrane module with 1 cm diameter membrane element.

6 Next steps

In the following year, we will

1. EPFL in collaboration with HES-SO has finished a demonstration site on campus which will be testbed for long-term stability testing of the membrane. We have also finished building a membrane skid (improved design (Figure 10) based on learning from pilot plant in GAZNAT Greengas initiative, Figure 60). We are now commissioning the membrane skid to test simulated flue gas from the waste incinerator. Our target is to establish long-term stability of membranes in a $CO_2/N_2/O_2$ mixture, and a mixture that contains 50 ppm NO_x and 5 ppm SO_x. The testing will be carried out using double-stage graphene membrane (50 cm^2 in size) with each condition tested for 1 month. The only exception is the condition regarding SOx and NOx which will be limited by the high cost of these custom gas bottles. For this, a week long test will be planned.
2. We are planning to bring the test skid to the site of Enevi. We have already made discussions and planning regarding the commissioning of the test skid next to the chimney in Enevi. Here, we will collect a month-long stability data from flue gas of waste-incinerator.
3. We will make a projection on the lifespan of the membrane based on the above results. As needed, we will study simulated flue gases for a longer period (beyond 4 weeks) to validate our stability prediction.

7 National and international cooperation

We have developed an improved process to transfer graphene allowing the process to be conducive to roll-to-roll fabrication (Bridge Proof of Concept and TeCH4Impact (by Dr. Mojtaba Chevalier as part of spinoff Divea), and EPFL internal funds). Here, we have already made 25 cm x 10 cm graphene coupons which show very good and consistent performance. For example, Figure 59 shows 250 cm^2 sized graphene membranes prepared by oxidation protocol developed under the SFOE project, and where graphene is successfully transferred to polymeric support. We have solved a number of challenges in this process with the biggest highlight being the whole process is simplified to allow the synthesis of graphene membrane by roll-to-roll process. For example, we do not anymore etch Cu foil (dissolving Cu foil) but rather simply peel off graphene from the Cu foil saving us time and making the process greener from the environmental point of view. The entire large membrane shows selective separation of CO_2 with performance parity from various sections of the membrane (Figure 59a and b). We have been also able to improve the membrane preparation method to avoid wrinkles in the membrane element further improving selectivity (from average 14 to 17, Figure 59c).

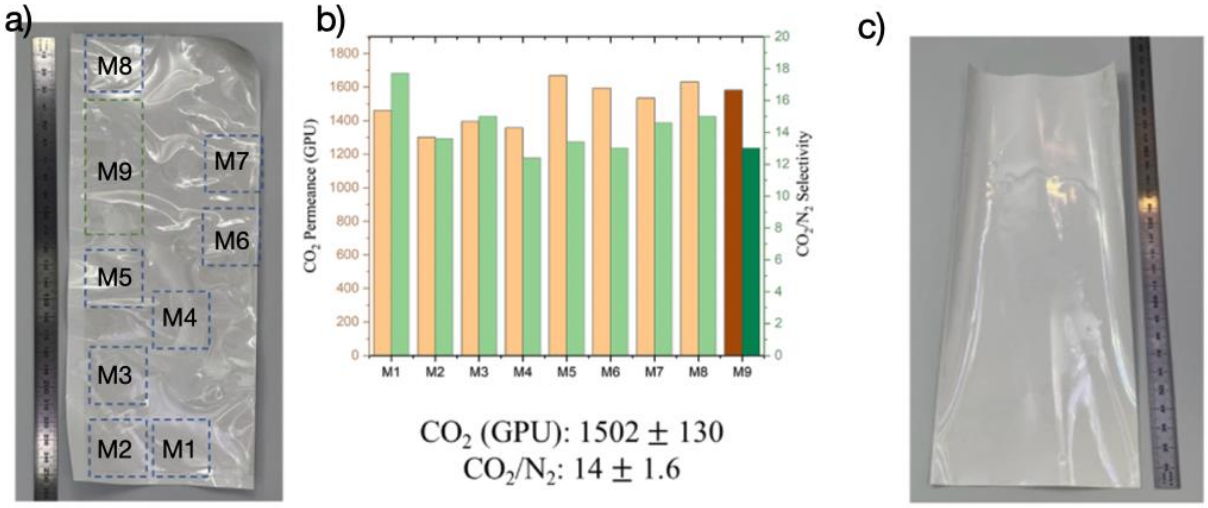

Figure 59. Recent developments in scaled-up production of graphene membrane (note: work funded by Bridge Proof of Concept, TeCH4Impact, and EPFL internal funding). Large-coupon of graphene membrane (10x 25 cm^2) resting on a porous polymeric support (a) and resulting performance from several coupons cut from this sample (b). c) Another large-coupon of graphene membrane (10 x 25 cm^2) where the adhesion between graphene and polymeric support is improved by avoiding the wrinkling of the support. As a result, the performance of graphene membrane has improved.

We have been also collaborating with GAZNAT for carbon capture from flue gas from CHP using natural gas (Figure 60). Under this project, we have built a membrane skid which shows extremely promising data for flue gas separation.

Figure 60. Membrane skid for testing graphene membranes for the separation of flue gas from combined heat and power (CHP), installed in Aigle under the premises of GAZNAT.

The results are highly encouraging showing excellent stability of membranes in the flue gas from CHP which contains 50 ppm NOx (Figure 61). The membrane has been operated for 3 weeks continuously

without any regeneration. The fluctuation in data is due to fluctuation in feed supply (CHP is not always on) where we are storing the flue gas in a pressurized tank.

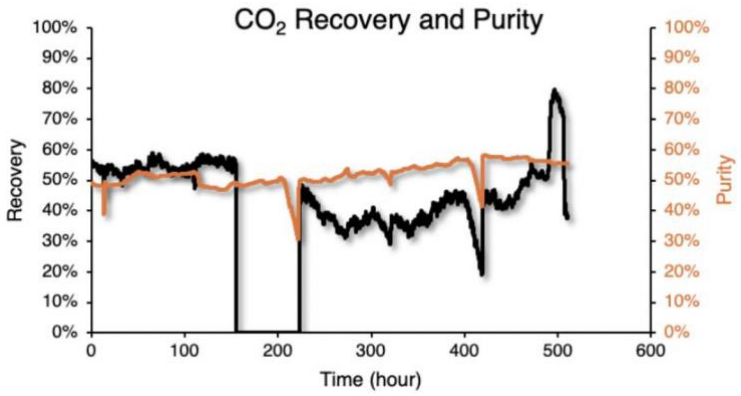

Figure 61. Recovery and purity data from single-stage graphene membrane (50 cm^2) separating flue gas from CHP containing 50 ppm Nox.

We have also received funding from EPFL on a project called Solutions4Sustainability to further scale-up graphene membrane by roll-to-roll technique in order to increase the capture capacity to 1 tonCO_2/day. The capture source will be Enevi waste incineration plant (same source as targeted in the SFOE project). A short summary of the project can be found at

https://www.epfl.ch/labs/las/solutions4sustainability/

8 Communication

There have been several communications on the scale-up activity of graphene membrane, especially under the scope of GAZNAT greengas project. These include:

(1) Agrawal, K. V.; Bautz, R. "Capture Du Carbone". *Aqua & Gas* **2022**, 46–53.

http://www.aquaetgas.ch/fr/énergie/gaz/20220225_capture-du-carbone/

(2) René Bautz; Gilles Verdan, Noris Gallandat; Liping Zhong, Andreas Züttel; Kumar Varoon Agrawal, "Greengas - projet gazier innovant". *Aqua & Gas* **2024**, 36–44.

https://www.aquaetgas.ch/fr/énergie/gaz/20241031-greengas-projet-gazier-innovant/

There have been several presentations at invited lectures at international conference as follows:

1. Interdisciplinary Perspectives on Transport Mechanisms in Membranes and Nanopores, France, 2025.
2. International Conference on Carbon Capture and Utilization 2024 (ICCCU24), India, 2024.
3. International conference From Solid-state to Biophysics XI, Croatia, 2024.
4. Materials Research Society (MRS) Spring Meeting, Nanoscale Mass Transport Through 2D and 1D Nanomaterials, USA, 2024.
5. Gordon Research Conference (GRC) on Nanoporous Materials and Their Applications, Proctor Academy, USA, 2023.

We have also made presentations (contributed) to international conferences including American Institute of Chemical Engineers (AIChE) 2024.

Finally, the progress has been disseminated in invited research seminar and research talk:

1. Research Talk, Center for Enhanced Nanofluidic Transport (CENT), August 2024.
2. Seminar, NTU Material Science Department, July 2024.
3. Research Talk, ETH Board, Lausanne, Switzerland June 2024.
4. Seminar, Yonsei University, Jan 2024.
5. Seminar, Tianjin University, Fall 2023.
6. Seminar, Suzhou University, Fall 2023.
7. Seminar, University of Texas at Austin, Fall 2023.
8. Seminar, Ohio State University, Fall 2023.
9. Seminar, IISC Bangalore, 2023.
10. Seminar, Shell, June 2023.
11. Seminar, Yonsei University, Jan 2023.

9 Publications

Some of the results indirectly and directly related to this project has been published here:

- Vahdat, Mohammad Tohidi, Shaoxian Li, Shiqi Huang, Carlo A Pignedoli, Nicola Marzari, and Kumar Varoon Agrawal. 2023. “Unraveling the Oxidation of a Graphitic Lattice: Structure Determination of Oxygen Clusters.” *Physical Review Letters* 131 (16): 168001. https://doi.org/10.1103/PhysRevLett.131.168001.
- Bondaz, Luc, Anshaj Ronghe, Shaoxian Li, Kristiāns Čerņevičs, Jian Hao, Oleg V Yazyev, K. Ganapathy Ayappa, and Kumar Varoon Agrawal. 2023. “Selective Photonic Gasification of Strained Oxygen Clusters on Graphene for Tuning Pore Size in the Å Regime.” *JACS Au*, September. https://doi.org/10.1021/jacsau.3c00395.
- Vahdat, Mohammad Tohidi, Shaoxian Li, Shiqi Huang, Luc Bondaz, Nicola Marzari, and Kumar Varoon Agrawal. 2023. “Mechanistic Insights on Functionalization of Graphene with Ozone.” *Journal of Physical Chemistry C*.
- Li, Shaoxian, Mohammad Tohidi Vahdat, Shiqi Huang, Kuang-jung Hsu, Mojtaba Rezaei, Mounir Mensi, Nicola Marzari, and Kumar Varoon Agrawal. 2022. “Structure Evolution of Graphitic Surface upon Oxidation: Insights by Scanning Tunneling Microscopy.” *JACS Au* 2 (3): 723–30. https://doi.org/10.1021/jacsau.1c00570.
- Huang, Shiqi, Luis Francisco Villalobos, Shaoxian Li, Mohammad Tohidi Vahdat, Heng-Yu Chi, Kuang-jung Hsu, Luc Bondaz, Victor Boureau, Nicola Marzari, and Kumar Varoon Agrawal. 2022. “In Situ Nucleation-Decoupled and Site-Specific Incorporation of Å-Scale Pores in Graphene Via Epoxidation.” *Advanced Materials* 34 (51): 2206627. https://doi.org/10.1002/adma.202206627.
- Agrawal, K. V.; Bautz, R. Capture Du Carbone. *Aqua & Gas*. 2022, pp 46–53.

- Hao, J.; Gebolis, P. M.; Gach, P. M.; Chevalier, M.; Bondaz, L. S.; Kocaman, C.; Hsu, K.-J.; Bhorkar, K.; Babu, D. J.; Agrawal, K. V. Scalable Synthesis of CO_2-Selective Porous Single-Layer Graphene Membranes. (2025, in press) Nature Chemical Engineering. https://doi.org/10.1038/s44286-025-00203-z.

10 References

[1] M. Bui, C. S. Adjiman, A. Bardow, E. J. Anthony, A. Boston, S. Brown, P. S. Fennell, S. Fuss, A. Galindo, L. A. Hackett, J. P. Hallett, H. J. Herzog, G. Jackson, J. Kemper, S. Krevor, G. C. Maitland, M. Matuszewski, I. S. Metcalfe, C. Petit, G. Puxty, J. Reimer, D. M. Reiner, E. S. Rubin, S. A. Scott, N. Shah, B. Smit, J. P. M. Trusler, P. Webley, J. Wilcox, N. Mac Dowell, *Energy Environ. Sci.* **2018**, 1062.

[2] E. S. Rubin, J. E. Davison, H. J. Herzog, *Int. J. Greenh. Gas Control* **2015**.

[3] T. C. Merkel, H. Lin, X. Wei, R. Baker, *J. Memb. Sci.* **2010**, *359*, 126.

[4] M. Micari, M. Dakhchoune, K. V. Agrawal, *J. Memb. Sci.* **2021**, *624*, 119103.

11 Appendix

Computational fluid dynamics (CFD) simulation

CFD simulations on the gas profile in the tubular furnace were performed using a COMSOL Multiphysics®6.1 package. The model geometry was created in the software. O_2 was selected as the fluid material. A laminar flow study was applied to the model, with a gas inlet and outlet specified on the left and right ends of the reactor. Other domains of the model were all defined as wall boundaries. The boundary condition for the inlet was set as a fully developed flow with a flow rate of 2 l/min, and that for the outlet was set as a static pressure of 0 Pa. The results were analyzed by COMSOL.